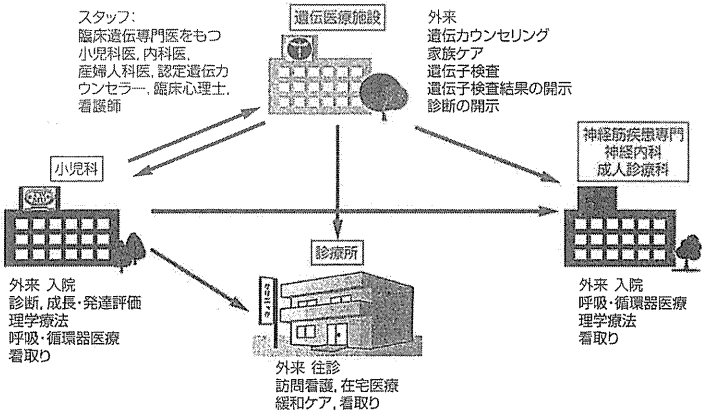

図3　神経筋疾患における移行医療

神経筋疾患における移行医療

図3に神経筋疾患における移行医療の具体的なパターンを示す．小児科では，疾患初期から成長・発達の評価を行うとともに，経過を診療し，必要に応じて理学療法，呼吸・循環器医療も実施する．そのなかで，疾患の重篤性や合併症により患児の最期を看取ることもありうる．神経筋疾患を有する患者において，小児科から神経内科や訪問看護を実施している診療所などの成人診療科への移行は，自身が疾患を受容して今後の身体的な状況に自ら対処していく心構えをもつという意味もある．

遺伝医療施設では，複数の臨床遺伝専門職（臨床遺伝専門医，認定遺伝カウンセラー，臨床心理士，看護師など）により，遺伝カウンセリング，家族ケア，心理カウンセリングなどの診療を行っている．小児科から成人診療科へのスムーズな移行において，これらの遺伝医療施設が，遺伝カウンセリングを通して，本人への診断の告知と，医療的・社会的・心理的サポート等の介入を行うことは意義があると考えられる．

文献　1）Hallum A:Disability and the transition to adulthood:Issues for the disabled child, the family, and the pediatrician. Current Problems in Pediatrics 25:12-50, 1995
2）Colver AF, et al.:Study protocol:Longitudinal study of the transition of young people with complex health needs from child to adult health services. BMC Public Health 13:675, 2013
3）Sawicki G, et al.:Receipt of health care transition counseling in the national survey of adult transition and health. Pediatrics 128:e521-e529, 2011
4）日本医学会：医療における遺伝学的検査・診断に関するガイドライン，2011年2月，2011

著者連絡先　（〒162-0054）東京都新宿区河田町10-22
東京女子医科大学附属遺伝子医療センター　斎藤加代子

Images in Child Neurology

立ち上がりにくい，ころびやすい7歳男児

主　訴　立ち上がりにくい，よくころぶ．

現病歴　定頸5カ月，寝返り7カ月，独歩1歳10カ月と運動発達遅延を認めていたが，精神発達は正常であった．4歳頃から，歩行時のつまずき，易転倒が目立つようになった．普通小学校に入学し，徒歩通学していたが，易疲労性，歩行不安定のため，ランドセルを背負っての通学はしていなかった．7歳時の患児を図1に示す．意識清明，脳神経・胸腹部に異常を認めなかった．両上肢の挙上は可能であったが，腰帯筋および近位筋優位の下肢筋力低下を認め，歩容は腰を突き出し動揺性であった．臥位からの立ち上がりでは，両手で膝を押さえ上半身を持ち上げていた（図1-①～④）．ジャンプは不可能であった．深部腱反射は保たれ，病的反射は認めなかった．膨らんだ腓腹部は硬く，時に同部の痛みを訴えた（図1-⑤）．

既往歴　特記すべきことなし．

家族歴　健常な弟が一人．同様の病状を呈する血縁者はいない．

問題1　疑われる疾患は？　その鑑別のために必要な検査は何か？

問題2　問題1で行った検査結果を踏まえて，次に行うことは何か？

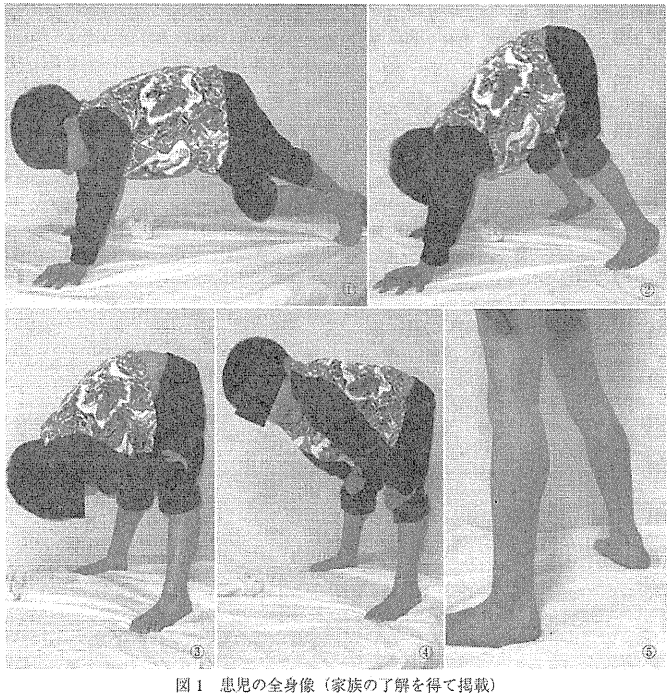

図1　患児の全身像（家族の了解を得て掲載）

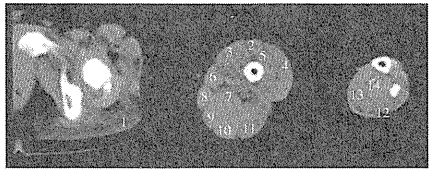

図2　腰帯・下肢筋CT（左側）
1：大臀筋，2：大腿直筋，3：内側広筋，4：外側広筋，5：中間広筋（2～5で大腿四頭筋），6：縫工筋，7：大内転筋，8：薄筋，9：半膜様筋，10：半腱様筋，11：大腿二頭筋（長頭），12，13：腓腹筋，14：ヒラメ筋
大臀筋，大腿四頭筋，大腿二頭筋，腓腹筋などに低吸収域を認める．

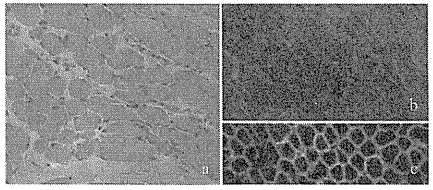

図3　左上腕二頭筋生検組織
a：H＆E染色，b：ジストロフィン染色，c：ジストロフィン染色正常コントロール（×200）
筋線維の大小不同，壊死・再生線維，筋線維間の結合組織増加を認める．ジストロフィン染色では筋線維膜は染色されない．

問題1の答え　血液検査で，血清クレアチンキナーゼ（CK）の値を確認する．

幼少期の運動発達遅延を呈する疾患は多種多様で，鑑別として筋ジストロフィー，先天性ミオパチー，神経原性筋萎縮症，脳性麻痺，先天代謝異常，染色体異常のほか，整形外科疾患なども挙げられる．鑑別のためには，運動発達歴の詳細な聴取，臨床症状評価に加え，血清CKを含む血液生化学検査，神経伝導速度検査や針筋電図検査など電気生理学的検査，中枢神経系や筋のCT，MRIなど画像検査が有用である．鑑別のうえ，遺伝子検査が可能な疾患の場合は遺伝子検査施行を検討する．遺伝子検査で診断に至らない場合，必要に応じ筋生検を行う．

本例の精神発達は正常で明らかな家族歴もなかったが，歩行獲得時期の遅延や登攀性起立（Gowers徴候，図1-①～④），腓腹部の仮性肥大（図1-⑤）を認めた．血清CKは15,000～20,000 IU/lと著しく上昇していた．血清CKが数千IU/lの場合，筋炎の可能性が否定出来ないこともあり，病状，臨床経過からの慎重な判断が求められるが，本例のようにさらに高値である場合，筋ジストロフィー，特にDuchenne/Becker型筋ジストロフィー（DMD/BMD）の可能性を最も考える．

図2に，本患児の腰帯・下肢筋CT画像を示す．DMD/BMDでは，共同筋間でも病変進行のスピードが異なるため，脂肪化した筋の間に変化の程度が軽い筋が混在するselectivity patternを呈す[1]．本症例では大臀筋，大腿四頭筋，大腿二頭筋などに加え，内眼的に肥大を認めた腓腹筋に低吸収域を認めた．一方，上肢・体幹の筋や，縫工筋，薄筋，半腱様筋，半膜様筋は保たれていた．

問題2の答え　遺伝子検査を含む確定診断を行うための検査の説明を行う．さらに，診断確定後は，疾患に関する正確な医学的情報を提供することに努める．

DMD/BMDの可能性が考えられた場合，診断のためには遺伝子検査を行うことが第一選択である[2]．現在は，multiple ligation-dependent probe amplification（MLPA）法による検査法が一般的で，ジストロフィン遺伝子のエクソン単位の欠失・重複の判定が可能である．MLPA法で変異が確認されない場合，確定診断のためには筋生検を行う．本症例ではMLPA法での変異が確認されなかったため，左上腕二頭筋で筋生検を行った．筋線維の大小不同，壊死・再生線維，筋線維間の結合組織増加を認め，ジストロフィン染色では筋線維膜は染色されず，DMDと確定診断した（図3）．のちに，本症例では，ジストロフィン遺伝子の1つのエクソンに1塩基置換の変異が確認された．

遺伝子検査実施にあたっては，遺伝カウンセリングの立場に基づいた十分な説明が必要である．血清CKが高値という理由だけで，安易に遺伝子検査を行うべきではない．DMDの遺伝子変異の3分の2は母由来であり，母の保因者診断，次子の妊娠などについても言及する必要がある．

DMDでは，幼少期からの積極的なリハビリテーション介入は必須である．運動機能維持のためのステロイド投与は，保険適応が承認された．呼吸不全に対する非侵襲的人工呼吸療法，心不全に対するβ遮断薬投与などの積極的治療介入で，DMDの平均余命は30歳を超えるまでに改善し，嚥下障害・栄養障害，腎不全といった，生命予後改善ゆえの新たな問題も発生してきている．また，ものごとへのこだわりや自閉傾向，発達障害傾向は，中枢神経でのジストロフィン欠失による症状である可能性が指摘され，新たな課題として認識されている．エクソンスキッピング療法をはじめとする国際共同試験，患者登録システムや臨床試験ネットワークの形成など，DMD治療に向けた新たな仕組み作りが進んでいる．

Key note

DMDを取り巻く治療環境は変わりつつあり，診断にとどまらず，診断後の長期にわたる対応が重要である．

文　献
1）川井　充，国本雅也，本吉慶史，桑田隆史，中野今治．Duchenne型筋ジストロフィー症の骨格筋CT所見とこれにもとづく病期分類．臨床神経 1985；25：578-90.
2）「神経疾患の遺伝子診断ガイドライン」作成委員会，編．神経疾患の遺伝子診断ガイドライン　2009．東京：医学書院，2009.

齊藤利雄
〒560-8552　大阪府豊中市刀根山5-1-1
国立病院機構刀根山病院神経内科・小児神経内科
E-mail：saitot@toneyama.go.jp
（受付日：2013. 2. 28，受理日：2013. 5. 2）

OPERATING MANIPULATOR ARM BY ROBOT SUIT HAL FOR REMOTE IN-CELL EQUIPMENT MAINTENANCE

ROBOTIC AND REMOTE SYSTEMS AND HUMAN FACTORS

KEYWORDS: *HAL robot suit, bioelectrical signals control, in-cell equipment maintenance*

AKIHIRO KITAMURA,[a]* TAKASHI NAMEKAWA,[a]
KOUSUKE HIRAMATSU,[b] and YOSHIYUKI SANKAI[b]

[a]*Japan Atomic Energy Agency, 4-33 Tokai, Naka, Ibaraki 319-1194, Japan*
[b]*University of Tsukuba, 1-1-1, Tennodai, Tsukuba, Ibaraki 305-8573, Japan*

Received January 6, 2013
Accepted for Publication March 27, 2013

A remote control system to operate a manipulator arm by the HAL (Hybrid Assistive Limb) robot suit is examined in the application of in-cell equipment maintenance. In this integrated system the operator wears the exoskeletal-structured HAL and the operator's movement is transferred through HAL's computer system to a slave-type manipulator arm. The system includes a bioelectrical signals (BES) control scheme and a position control scheme. In the former scheme, sensors attached to the skin on the operator's arms detect faint BES when the operator makes a movement. The signals are processed and analyzed by a computer to determine the operator's intention. The computer then calculates the necessary assistive power and the power units generate adequate power to each joint of the HAL suit to assist the operator. To evaluate the effectiveness and usefulness of the system, remote handling experiments were designed using mockup equipment, and the performance of remote operation conducted by the two schemes mentioned above was compared with that by the more conventional three-dimensional mouse control scheme. Of these three control schemes, the BES control scheme clearly outperformed the others in executing direct-contact tasks of in-cell equipment maintenance with small operation time and small variation.

I. INTRODUCTION

Management of radioactive waste, including the spent fuel from the nuclear fuel cycle containing plutonium and minor actinide isotopes, is a pressing issue because of well-founded concerns over long-term safety, radiotoxicity, and heat generation. The development of minor actinide processing technologies therefore is receiving increasing interest because it could help to reduce the volume of radioactive waste destined for geological disposal, enhance proliferation resistance of the nuclear fuel cycle, and increase the efficiency of natural resource utilization.[1] Conversion of transuranic (TRU) elements such as plutonium, neptunium, americium, and curium into nuclear reactor fuels is considered to be one of the options in both existing and future nuclear fuel cycles, and the Japan Atomic Energy Agency (JAEA) is implementing research on the thermal properties of minor actinide oxides.[2–5]

Fabrication of low-decontaminated TRU fuels on the large scale requires more remote operability and maintenance performance than conventional glove-box-type processing due to the high radiation exposure. The fuel fabrication equipment is also expected to have high precision. To meet the above demands, the Advanced Nuclear System Research and Development Directorate of JAEA proposed a module-type in-cell fuel fabrication equipment system. The repairing and maintenance scheme of the system currently considered consists of three stages[6]:

1. Replace the out-of-order module in the main process cell.

2. Decontaminate and disassemble the module in the maintenance cell.

3. Repair the module using the glove box in the maintenance room.

*E-mail: kitamura.akihiro@jaea.go.jp

To confirm the adaptability of this proposed equipment system, representatives of in-cell equipment such as pressing machine, pellet inspection equipment, and powder analyzer were designed and fabricated. A series of mockup experiments were made to confirm the process of replacing the out-of-order module in the main process cell.[7] A similar prototype assembly for nuclear fuel reprocessing has been described elsewhere.[8,9]

There is an important need for remote operating systems in a number of industrial settings, including hazardous, toxic, or constricted workspaces that are mostly inaccessible for humans. Currently in Japan, the most urgent need for a remote operating system is in the cleanup of the Fukushima nuclear power plant. Several prototype remote operating systems have been developed: the Auto Blaster system of Tharr developed for bridge maintenance,[10] the HydrCat of Lorenc et al. for removing coatings from structures in marine and nonmarine industries,[11] the crawling robots of Ross et al. for buildings or storage tanks,[12] and a large robotic paint-stripping system introduced by Schmitz for aircraft maintenance.[13] Remote operating systems implemented in maintenance, decommissioning, and waste management of nuclear fields include teleoperated manipulators developed by the Oak Ridge National Laboratory and the University of Tennessee[14]; a vitrification facility dismantlement project undertaken at West Valley, New York[15]; remote glove-box size reduction performed by JAEA (Ref. 16); robotics research and development conducted by the Commissariat à l'Énergie Atomique et Aux Énergies Alternatives[17]; and a waste packaging robotic welding and inspection system demonstrated by the Idaho National Laboratory.[18,19] Recently, CYBERDYNE announced that the robot suit HAL (Hybrid Assistive Limb) invented by Sankai Laboratory of the University of Tsukuba could be used in dismantling the Fukushima nuclear plant. The suit is designed to assist workers who need to wear cumbersome personal protective clothing and to provide better shielding against radiation.[20,21]

To execute remote operational tasks in an efficient manner, it is necessary to select the correct type of remote control terminals for specific task requirements. Button- or switch-type controllers transfer the programmed movements to the robotics and are widely used in repetitive tasks. Joystick controllers apply potentiometric, inductive, or photoelectric sensing systems and/or switches to translate joystick motion into an output signal and are used for steering, positioning, and speed control. Master-slave–type controllers transmit the motion from the master part to the slave part and are adequate for posture control and material handling. A three-dimensional (3-D) mouse transforms its movements by pushing, pulling, and/or twisting to the robotics and is used in a variety of fields including computer-aided design applications, 3-D modeling, animation, 3-D visualization, and product visualization. The appeal of a 3-D mouse over a conventional mouse and keyboard is the ability to pan, zoom, and rotate 3-D imagery simultaneously, without stopping to change directions using keyboard shortcuts or a software interface.

Although these controllers are used for a variety of tasks, transferring the sensitive intention of the operator to the slave arm is still a very challenging field to be explored. In the current study, a remote control system is introduced to operate a manipulator arm for in-cell equipment maintenance by the robot suit HAL. The system includes a bioelectrical signals (BES) control scheme and a position control scheme. In the former, sensors attached to the skin of the operator's arm detect faint BES when the operator makes a movement. The signals are processed and analyzed by a computer to determine the operator's intention. The computer then calculates the necessary assistive power and the power units generate adequate power to the HAL suit to assist the operator. In the position control scheme, the slave arm traces the path of the operator's movements as in the BES control scheme, but no assistive power is supplied. To evaluate the effectiveness and usefulness of such a remote control strategy, remote handling experiments were undertaken using a mockup of the equipment found in the main process cell. The performance of the remote operation conducted by the present two control schemes was compared with that by the more conventional 3-D mouse control scheme.

II. SYSTEM CONFIGURATION

The master-slave–type manipulation system integrated in this study consists of the HAL robot suit and a manipulator arm. An operator who wears HAL controls the posture and movement of HAL. A manipulator arm is controlled by HAL and performs the intended tasks in the workspace remotely. A Mitsubishi PA-10 robot arm was chosen as the slave manipulator arm (Fig. 1); it has seven degrees of freedom (DOF) and an open control architecture and is manufactured by Mitsubishi Heavy Industries (MHI). The four-layer control architecture is made up of the robot arm, servo controller, motion control card, and upper control computer.

In a highly radioactive environment, components of the robot arm are required to have adequate radiation resistance,[22] in particular the ac servo motor, cables, electronic devices, and position sensors.[23–26] Although such modifications have not been implemented or tested here, a mobile robot with dual robot arms that provides enhanced radiation protection, including anticontamination measures, has been recently developed by MHI (Ref. 27), and thus the test results achieved in the current study are not expected to differ qualitatively.

HAL is a powered exoskeletal robot suit created by Sankai Laboratory of the University of Tsukuba to expand and improve the physical capabilities of humans.[28–32] The HAL we utilized in this study is an upper limb type

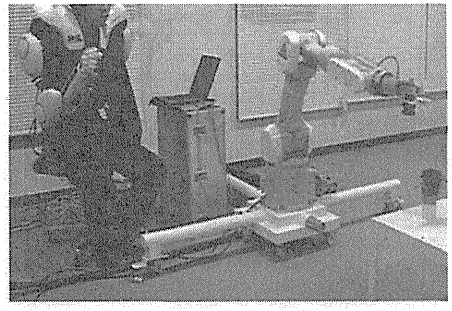

Fig. 1. System overview of the integrated master-slave manipulation system. Exoskeletal robot suit HAL invented by Sankai Laboratory of the University of Tsukuba and PA-10 manufactured by MHI are utilized as master arm and slave arm, respectively.

and consists of frames to support the operator's upper body, power units (actuators including motors) installed at joints of elbows and shoulders, sensors to detect the BES on the operator's skin surface, angle sensors, posture sensors, force sensors, wireless LAN, batteries, and a computer to control the system. The HAL exoskeleton powers the flexion/extension joints at the elbow and wrist via a dc motor with harmonic drive placed directly on the joints. The torque of the power units is converted from HAL to a wearer's limb through the mold fastening equipment. To assist the motion of an operator and to perform force feedback, HAL uses two DOF in a shoulder joint and one DOF in an elbow joint.[33,34]

Since intensive bilateral data communication between the HAL system and the PA-10 system is indispensable, the following protocols are adopted for processing the data between the systems:

1. To synchronously equate the direction and the movement of the end effectors of HAL and PA-10, the position coordinate data of the end effectors are adopted instead of the joint angle data of HAL and PA-10; the length of the arm components and the joint structures of HAL and PA-10 are different (the ranges of rotating motion as well), so one-to-one correspondence of the posture of HAL and PA-10 is not possible. The position coordinate data capture scheme makes bilateral communication accurate even though the structures of the master and slave arms are not equivalent.

2. For collision control strategy, a relative coordinate value of the migration length of the end effector was used instead of the absolute coordinate value of the end effector position. The reason for choosing this scheme is to remove the possibility of large movement of the end effector that might occur in the absolute coordinate value–based control scheme (if error is included in the received data). This collision avoidance mechanism enhances the sensitivity of the end effector movements as well.

3. For the interactive communications between HAL and PA-10 systems, a user datagram protocol (UDP) is adopted instead of transmission control protocol (TCP), because UDP has shorter transfer time and smaller data reception than TCP.

When the operator wearing a HAL suit moves his or her arm, the posture information of HAL is transferred to a control system to move the manipulator arm instantaneously. In addition to such tight integration of the HAL and manipulator arm mechanisms, the system can also treat BES in the control loop, which plays a vital role in remote operation[33,34]; hereafter we refer to this as the BES control scheme.

The block diagram of the whole master-slave system is depicted in Fig. 2. The human operator block refers to the operator, while the HAL block refers to HAL itself, including its control system. The cybernic master arm joints block corresponds to the operator's arm joints and the power units embedded in HAL. The slave arm block here represents the robot arm PA-10. In the human operator block "controller of human" corresponds to the operator's recognition and decision and "musculoskeletal system" corresponds to the operator's intention of movement and resulting musculoskeletal movement.

The operator's movement is transmitted as torque, τ_{human}, to the cybernic master arm joints. The resulting posture information, i.e., joint angle data θ_m, is sent to the HAL system to generate the movement of PA-10, Xm, by calculating forward kinematics FK. Simultaneously, θ_m is sent back to the operator with force feedback τ, composed of τ_{CMA} (described below) and τ_{human}. The resulting movement of PA-10, Xs, is traced back to the system and the deviation of Xm and Xs is evaluated by calculating inverse kinematics IK, and an adequate torque τ_X that minimizes the deviation of Xm and Xs is determined in A, and corresponding force feedback gain is then processed via Kp. Similarly, the force applied at the tip of the end effector, Fs, is captured by the force sensor; torque τ_F necessary to avoid overload is calculated in JT; and the corresponding force feedback gain is processed via Kf.

In the BES control scheme, sensors attached to the skin on the operator's arms detect faint BES transmitted from the brain to muscle tissue when the operator makes a movement. The signals V are processed and analyzed by a computer to determine the operator's intention. The computer successively calculates the necessary assistive power τ_{hal} for HAL. This value is combined with the aforementioned force feedback gains to determine the optimum assist torque τ_{CMA}, and the power units generate suitable power to each joint of the HAL suit to assist the operator.

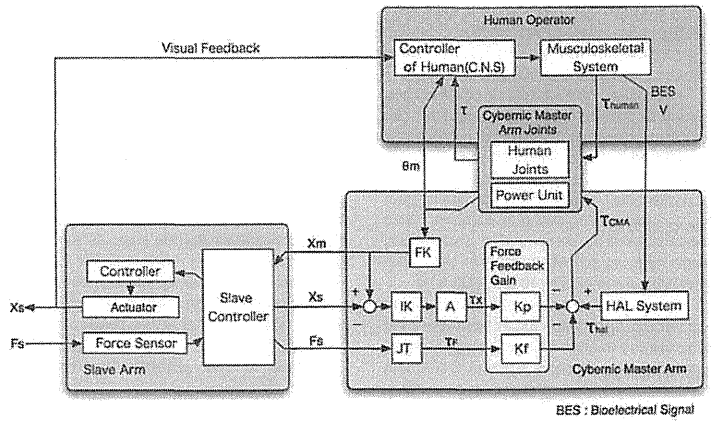

Fig. 2. Block diagram of the integrated system. Notation used in the figure is described in the text.

Furthermore, the present control loop includes visual feedback; the operator can observe either directly or indirectly (through cameras or computer-aided graphics on monitors) the workspace to make necessary adjustments to the movement of the PA-10.

The speed of HAL's actions (detection, calculation, and generation) exceeds the time of musculoskeletal actions, and therefore, significant reductions of the system's control loop latency and the operator's workload are attained. In the position control scheme, the slave arm traces the path of the operator's movements and the force feedback is reflected from the slave arm as in the BES control scheme; however, no assist torque is generated from the HAL system.

III. EXPERIMENTAL SETUP

To evaluate the efficiency and usability of the integrated HAL and PA-10 system, remote maintenance experiments were undertaken using mockup equipment, consisting of a pressing machine, pellet inspection equipment, and powder analyzer. Of these, the pressing machine may be considered the most complex in terms of the number of modules and maintenance mechanisms that must be performed, so it was chosen as the most rigorous test in the current study.[35]

Basic remote handling units of the pressing machine are the pins to lock and unlock the hanger for equipment removal and reinstallation; connectors to engage lines for supply of gas, liquid (which is similar to the gas supply connector and therefore omitted from this test bed), and electricity; and bolts to fasten and unfasten modules and submodules in various places (Fig. 3). The sequence of the remote operational tasks required in the removal and reinstallation of a module is as follows:

Removal of modules:

1. Unlock two left-side lock pins to disconnect the module equipment and the framed hanger by moving down the lock pins from a horizontal position.

2. Unlock two right-side lock pins to disconnect the module equipment and the framed hanger by moving down the lock pins from a horizontal position.

3. Remove the framed hanger from the module equipment by moving up the crane.[a]

4. Disengage the compressed gas supply connector by pressing and moving down the connector.

5. Disengage the electricity supply connector by pressing and moving down the connector.

6. Attach an impact driver to the manipulator arm by closing the gripper.[b]

7. Insert the cusps of the impact driver to the bolt to unfasten the bolt by shifting the robot arm.

8. Detach the impact driver from the manipulator arm by opening the gripper.[b]

[a] Tasks using the crane were not performed in this experiment.
[b] Since we have not made a tool-exchanging equipment, actual remote operations for exchange of the tool were not performed.

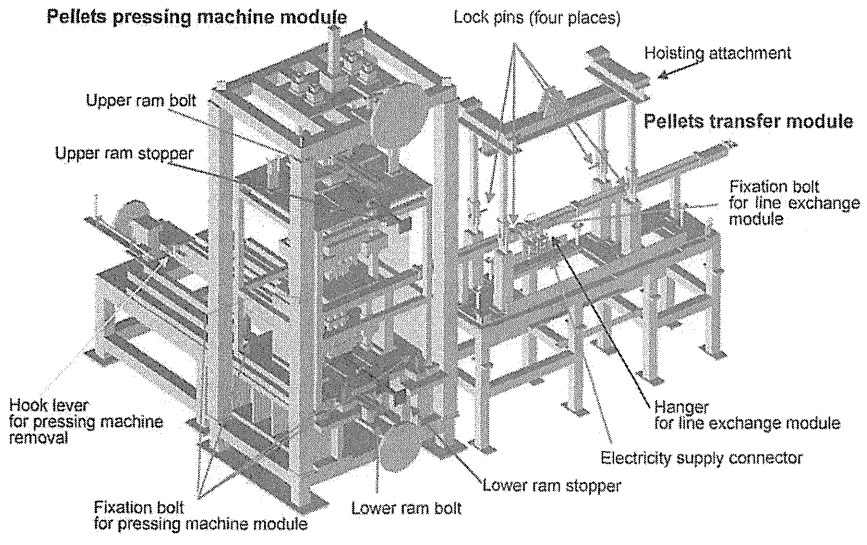

Fig. 3. Access points in mockup equipment required for remote operation. Basic remote handling units are the pins to lock and unlock the hanger for equipment removal and reinstallation; connectors to engage lines for supply gas, liquid, and electricity; and bolts to fasten and unfasten modules and submodules (exchange module) in various places.

9. Hold the submodule (a line-exchange equipment) by inserting the end effector of the arm to the hanger of the submodule.

10. Detach the submodule (the line-exchange equipment) from the module equipment by lifting up the arm.

11. Remove the submodule to a repair shop by moving out the arm.

12. Connect the framed hanger to the module equipment by bringing down the crane.[c]

13. Separate the module equipment by lifting up the crane.[c]

14. Transfer the module equipment to the repair cell by moving out the crane.[c]

Reinstallation of modules:

15. Locate the repaired module equipment to the set position by shifting the crane.[c]

16. Reinstall the repaired module equipment by bringing down the crane.[c]

17. Locate the repaired submodule (the line-exchange equipment) to the set position by shifting the arm.

18. Reinstall the repaired submodule (the line-exchange equipment) by bringing down the arm.

[c]See footnote a on p. 313.

19. Engage the compressed gas supply connector by supporting the flange of the connector from the bottom and moving up the bottom part of the connector.

20. Engage the electricity supply connector by supporting the flange of the connector from the bottom and moving up the bottom part of the connector.

When bringing down the module equipment with the framed hanger (process 12 in removal of modules), the lock pins are automatically locked by a systematic mechanism. Thus, we do not need to lock the pins by remote arm operation. Disengaging and engaging the electric connector were found to be the most difficult among these tasks, because the system is designed for a nuclear use with a complex set of holes and corresponding pins with tight tolerances. The tasks of removal and reinstallation of the submodule were also found to be difficult, requiring delicate control and sharp movements to accomplish.

The required goals in this in-cell remote equipment maintenance development were that the replacement of the module should be completed within 6 h and that the execution of an individual task can be performed repeatedly. The time taken to transfer the module by crane and to exchange the tool by remote robot arm is also included. By excluding these tasks, the time requirement for removal and reinstallation tasks to be completed by the remote robot arm is reduced to ~1 h. Several identical modules are meant to be ready for use. Thus, when one module equipment is out of order, an already repaired module is ready for replacement, and we ignore the repairing time for out-of-order module equipment.

The three control schemes we have adopted for evaluation in this study are as follows.

1. *BES control scheme:* The operator wears the HAL suit and moves his or her arm to control the remote robot arm. As the operator's arm moves, the position of the end effector of the robot arm traces the path. After the positioning of the end effector is settled, a cyber glove is used to open and close the end effector of the arm to operate the object with additional adjustment, as necessary, by movement of the operator's arm. BES signals are processed and analyzed by a computer to determine the operator's intention. The necessary assistive power is calculated by the computer and the adequate power is generated by the power units (see details in Sec. II).

2. *Position control scheme:* The operator wears the HAL suit and moves his or her arm to control the remote robot arm as in (1). In this scheme, however, the optimal assistive power is not generated to assist the operator.

3. *3-D mouse control scheme:* The operator moves the controller cap of the 3-D mouse to control the remote robot arm. In the current study, a SpaceNavigator from 3Dconnexion was used.[36] By leaning the controller cap to the left, right, forward, or back, the end effector (gripper) of the robot arm simultaneously moves to left, right, forward, or back, or by pulling the controller cap up or down, the end effector (gripper) of the arm simultaneously makes the same movement. Increase pressure to go faster and make large movements or reduce pressure to go slower and make fine adjustments. After the positioning of the end effector is essentially complete, a button-type controller is used to open (release) and close (grip) the end effector to manipulate the object along with any further adjustments, as necessary, by 3-D mouse control.

IV. RESULTS AND DISCUSSION

To evaluate the performance of the integrated HAL and PA-10 system directly, a remote handling experiment in the vicinity of the test bed with direct observation was first conducted, as shown in Fig. 4. A cyber glove was worn by the operator, for (open and close) manipulation of the end effector (Fig. 5). The experiment was performed by the BES control scheme. Using this control scheme, far less time was taken to perform a number of individual tasks in comparison with the more conventional schemes:

1. Time required to insert the bolt was found to be ~8 s.

2. Time required to remove the submodule equipment was found to be ~20 s.

3. Time required to disengage the supply gas connector was found to be ~7 s; time required to engage the supply gas connector was found to be 17 s.

4. Time required to disengage the electrical connector was found to be ~9 s; time required to engage the electrical connector was found to be 24 s.

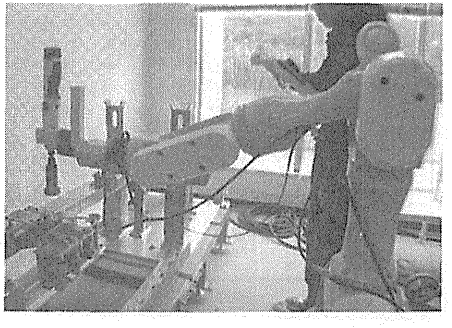

Fig. 4. Remote handling experiment in the vicinity of the test bed with direct observation.

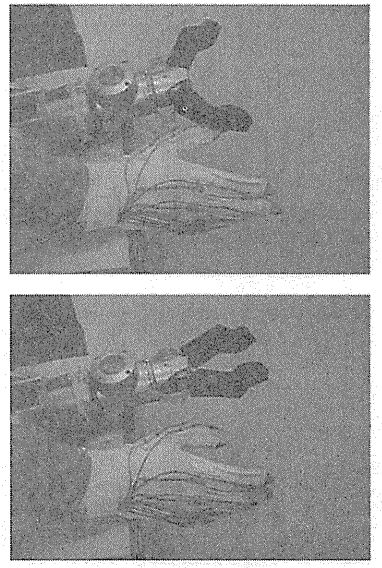

Fig. 5. The cyber glove used for end effector (gripper) manipulation. The cyber glove possesses 5 DOF but is here restricted to 2 DOF for the purpose of grip and release.

It was confirmed that the system convincingly controls the end effector of the slave arm and manipulates sensible tasks, such as handling the unstable thin hanger of the submodule equipment and treating the tight connectors.

In the comprehensive mockup experiment, a course of tasks is repeated in triplicate using each control scheme (HAL with BES control scheme, HAL with position control scheme, and 3-D mouse control scheme). The operator in the remote operation booth with monitors providing instant feedback information is shown in Fig. 6. In Fig. 7, remote operation times required to complete the series of tasks for mockup equipment are shown. The required goals were attained in all three control schemes. As can be seen from Fig. 7, the times to complete the total remote operation task by the HAL system with the BES and the position control schemes were both smaller than that by the 3-D mouse control scheme. In the HAL system with the BES control scheme, the time to complete the total task was about two-thirds that of the 3-D mouse control scheme. The variation of the time to complete all the tasks was also smaller in the BES control scheme. Although the variation of the time to complete the tasks becomes smaller as the operator gains experience, this index explains the effectiveness of the control schemes to some extent.

Fig. 6. The remote operation booth in the comprehensive test.

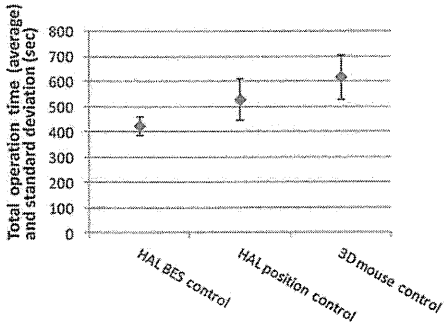

Fig. 7. Total remote operation time (average) and deviation in each experiment.

Results from individual tasks are shown in Table I. We observe that in almost all cases, the times and the variances to complete individual tasks were smaller in the HAL system with BES control scheme. The variance of time taken to disengage the electrical supply connector (which has many sockets and is tighter than the air supply connector, as mentioned earlier) by this control scheme was about one-fourth of that by the 3-D mouse control scheme. Very small variations of the time were also observed for the tasks of detaching and removing the line-exchange equipment and of engaging the electrical supply connector in the BES control scheme. These results suggest that the HAL system with BES control scheme is an improvement on the man-machine interface and is better suited to the current experimental conditions than other, more conventional methods.

In terms of operability, the following features were found from this experiment:

TABLE I

Average Times and Variances to Complete Individual Remote Operations in Three Control Schemes

Remote Procedure	Control Scheme		
	HAL with BES Control (s)	HAL with Position Control (s)	3-D Mouse Control (s)
Removal of modules			
Unlock two left-side lock pins	28 (8)[a]	28 (25)	53 (18)
Unlock two right-side lock pins	58 (21)	68 (8)	65 (17)
Disengage the compressed gas supply connector	71 (11)	78 (12)	72 (17)
Disengage the electricity supply connector	25 (5)	34 (7)	58 (20)
Insert the cusps of the impact driver to the bolt	74 (20)	86 (40)	94 (24)
Hold the submodule (line-exchange equipment)	32 (4)	46 (5)	50 (3)
Detach the submodule	5 (2)	5 (0)	13 (12)
Remove the submodule to a repair shop	5 (1)	6 (2)	17 (1)
Reinstallation of modules			
Locate the repaired submodule	10 (3)	11 (7)	17 (4)
Reinstall the repaired submodule	32 (20)	35 (37)	34 (22)
Engage the compressed gas supply connector	57 (12)	81 (17)	81 (8)
Engage the electricity supply connector	29 (8)	52 (36)	63 (17)
Overall	426 (38)	529 (83)	619 (87)

[a]Parentheses indicate variances.

1. In the 3-D mouse control scheme, the operator must operate three axes of direction simultaneously, depending on the mission situation. To operate the 3-D mouse properly, the operator must practice to gain skills in controlling the fingertip manipulation for the three axes direction, and it takes time to become used to it. It should be noted here that the operation of a manipulator arm in only one axial direction is, however, simple and gives sharp movement. Also, the lack of force feedback from the slave arm inhibits the performance of the operator because extreme caution is necessary to avoid collision/accidents during operation.

2. On the other hand, in using the exoskeletal-structured HAL system, one can operate the remote arm intuitively through a continuous feeling of the force feedback in the operator's arm and provide the necessary compliance for force feedback in direct-contact operation. In the position control scheme, however, the characteristics of the slave arm impedance and that of the HAL itself are superimposed, and these impedances are transferred directly to the operator. This drawback debilitates the operability of the system. In other words, the operator's discomfort and fatigue increases through the continued use of the HAL system.

3. Using the system with the BES control scheme, the HAL system reacts before the operator's full arm displacement occurs and therefore helps to ameliorate the above disadvantages. In the BES control scheme, even if the superimposed characteristics are transferred to the HAL system, the system cleverly removes these burdensome impedance characteristics, because in this scheme the operator is not required to move his or her arm but only to express the intention of action, to generate the assistive power of HAL. As a result, the efficiency of the operation is enhanced.

Through a thorough examination, the following items were recognized by the operator for the HAL with BES control scheme:

1. Smooth movement of the operator's arm is realized.

2. Oneness is obtained because the slave arm moves synchronously with the operator's arm.

3. Focus on the task during operation could be achieved while being less conscious of collision avoidance.

4. Appreciation of tiredness can be realized by adjusting the assist ratio and is valuable information from a health physics point of view.

5. Adequate movement is realized for large-space movement and sensitive procedures.

6. The operator could move around during operation because it is not necessary to sit or stand in one place. This helps to relieve operator stress and mitigate irritation.

7. Active use of BES in the impedance control system enhances an intuitive operational feeling.

V. CONCLUSION

A remote control system to operate a manipulator arm by the HAL robot suit is examined for the purpose of in-cell equipment maintenance. Two control schemes, a BES control scheme and a position control scheme, have been implemented. In the BES control scheme, sensors detect the operator's BES, a computer analyzes the intention of movement and calculates the necessary assistive power, and the power units generate power to provide HAL to assist the operator. Performance of the two schemes was evaluated in comparison with a more conventional 3-D mouse control scheme using mockup equipment.

Among these three control schemes, the BES control scheme outperformed the others in terms of the amount of time taken to complete a series of equipment maintenance tasks, with small variance. In addition, the system appropriately reflected the operator intention and satisfactorily generated suitable power to assist the operator.

In conclusion, the experimental test results suggest that through the power-assisted design of the HAL suit mechanism, the BES control scheme of the system has very promising performance, offering a significant improvement over more conventional counterparts. Furthermore, the system provides flexible features that facilitate the remote maintenance of in-cell equipment that requires precision and dexterity.

ACKNOWLEDGMENTS

We would like to thank T. Okada, K. Nakai, M. Watahiki, T. Hosogane, and H. Hirano for contributing to this work in various stages; Y. Yamada and T. Uchida for providing the mockup equipment; Y. Onishi and K. Kawaguchi for helpful discussions; and C. Walker for reviewing the manuscript. The present study includes a part of the result of the Development of In-Cell Remote Equipment project entrusted to JAEA by the Ministry of Education, Culture, Sports, Science and Technology of Japan.

REFERENCES

1. "Status of Minor Actinide Fuel Development," NF-T-4.6, International Atomic Energy Agency (2009).

2. T. NISHI et al., "Thermal Conductivity of Neptunium Dioxide," *J. Nucl. Mater.*, **376**, 78 (2008).

3. A. ISHIMI et al., "Post Irradiation Examination Results of MA Containing MOX Fuel; Non-Destructive Examination Results of the Fuel Pins," JAEA-Technology-2009-003, Japan Atomic Energy Agency (2009).

4. K. MINATO et al., "Thermochemical and Thermophysical Properties of Minor Actinide Compounds," *J. Nucl. Mater.*, **389**, 23 (2009).

5. K. TANAKA et al., "Preparation and Characterization of the Simulated Burnup Americium-Containing Uranium-Plutonium Mixed Oxide Fuel," *J. Nucl. Mater.*, **420**, 207 (2012).

6. H. FUNASAKA, H. NAKAMURA, and T. NAMEKAWA, "Current Status on Fuel Cycle System of Fast Reactor Cycle Technology Development (FaCT) Project in Japan," *Proc. 16th Pacific Basin Nuclear Conf.*, Aomori, Japan, October 13–18, 2008.

7. T. NAMEKAWA et al., "Handling Technology of Low Decontaminated TRU Fuel for the Simplified Pelletizing Method Fuel Fabrication System," *Proc. Int. Conf. Fast Reactors and Related Fuel Cycles: Challenges and Opportunities (FR09)*, Kyoto, Japan, December 7–11, 2009.

8. J. D. LAW et al., "Advanced Remote Maintenance Design for Pilot-Scale Centrifugal Contactors," *Nucl. Technol.*, **173**, 191 (2011).

9. D. H. MEIKRANTZ et al., "A Centrifugal Contactor Design to Facilitate Remote Replacement," *Nucl. Technol.*, **173**, 289 (2011).

10. D. THARR, "Automated Abrasive Blasting Equipment for Use on Steel Structures," *Appl. Occup. Environ. Hyg.*, **15**, 713 (2000).

11. S. J. LORENC, B. E. HANDLON, and L. E. BERNOLD, "Development of a Robotic Bridge Maintenance System," *Automat. Constr.*, **9**, 251 (2000).

12. B. ROSS, J. BARES, and C. FROMME, "A Semi-Autonomous Robot for Stripping Paint from Large Vessels," *Int. J. Robot. Res.*, **22**, 617 (2003).

13. W. SCHMITZ, "Robotic Paint Stripping of Large Aircraft—A Reality with the FLASHJET® Coatings Removal Process," *Proc. Aerospace Coating Removal and Coatings Conf.*, Colorado Springs, Colorado, May 22–24, 2003.

14. R. HAMEL, "Human Interaction with Robots Working in Complex and Hazardous Environments," presented at Colloquium on Robotics and Automation, Naples, Italy, December 18, 2006.

15. M. J. CAIN, C. DAYTON, and A. M. AL-DAOUK, "Dismantling the Vitrification Facility at the West Valley Demonstration Project," *Radwaste Solutions*, March/April 2005, p. 36.

16. A. KITAMURA, M. WATAHIKI, and K. KASHIRO, "Remote Glovebox Size Reduction in Glovebox Dismantling Facility," *Nucl. Eng. Des.*, **241**, 999 (2011).

17. J. M. DETRICH, "Innovations in Dismantling Robotics," *Nucl. Eng. Des.*, **182**, 267 (1998).

18. C. I. NICHOL et al., "Yucca Mountain Waste Package Closure System Robotic Welding and Inspection System," *Nucl. Technol.*, **176**, 138 (2011).

19. K. SKINNER, G. HOUSLEY, and C. SHELTON-DAVIS, "A Fruit of Yucca Mountain: The Remote Waste Package Closure System," *Nucl. Technol.*, **176**, 296 (2011).

20. L. GREENEMEIER, "Robotic Exoskeletons from Cyberdyne Could Help Workers Clean Up Fukushima Nuclear Mess," *Sci. Am.* (Nov. 9, 2011).

21. CYBERDYNE Web site: http://www.cyberdyne.jp/english/ (current as of Jan. 6, 2013).

22. K. SHIBANUMA and T. HONDA, "ITER R&D—Remote Handling Systems: Blanket Remote Handling Systems," *Fusion Eng. Des.*, **55**, 249 (2001).

23. K. OBARA et al., "Irradiation Tests of Critical Components for Remote Handling System in Gamma Radiation Environment," JAERI-Tech-96-011, Japan Atomic Energy Research Institute (1996).

24. A. ITOH et al., "Development of Radiation-Hard Electric Connector with Ball Bearing for In-Vessel Remote Maintenance Equipment of ITER," JAERI-Tech-97-065, Japan Atomic Energy Research Institute (1997).

25. K. OKA et al., "Development of Radiation-Hard Components for Remote Maintenance," *J. Plasma Fusion Res.*, **73**, 69 (1997) (in Japanese).

26. N. TAKEDA et al., "Current Status of Research and Development on Remote Maintenance for Fusion Components," *J. Plasma Fusion Res.*, **84**, 100 (2008) (in Japanese).

27. "MHI Develops 'MEISTeR' Disaster Recovery Support Robot with 2 Arms Enabling Light-Duty Work Tasks," Mitsubishi Heavy Industries Web site: http://www.mhi.co.jp/en/news/story/1212121603.html (Dec. 12, 2012) (current as of Jan. 6, 2013).

28. Sankai Laboratory Web site: http://sanlab.kz.tsukuba.ac.jp/en/ (current as of Jan. 6, 2013).

29. S. LEE and Y. SANKAI, "Virtual Impedance Adjustment in Unconstrained Motion for Exoskeletal Robot Assisting Lower Limb," *Adv. Robotics*, **19**, 773 (2005).

30. K. SUZUKI et al., "Intention-Based Walking Support for Paraplegia Patients with Robot Suit HAL," *Adv. Robotics*, **21**, 1441 (2007).

31. H. SATOH et al., "Transferring-Care Assistance with Robot Suit HAL," *Trans. Jpn. Soc. Mech. Eng. C*, **76**, 227 (2010) (in Japanese).

32. A. TSUKAHARA et al., "Sit-to-Stand and Stand-to-Sit Transfer Support for Complete Paraplegic Patients with Robot Suit HAL," *Adv. Robotics*, **24**, 1615 (2010).

33. K. HIRAMATSU and Y. SANKAI, "Development of Manipulation System with Cybernic Master Arm Based on BES," *Proc. Joint 5th Int. Conf. Soft Computing and Intelligent Systems and 11th Int. Symp. Advanced Intelligent Systems (SCIS&ISIS 2010)*, Okayama, Japan, December 8–12, 2010.

34. K. HIRAMATSU and Y. SANKAI, "Proposal for Manipulation System with Cybernic Master Arm Based on BES Variable Impedance Control," *Trans. Jpn. Soc. Mech. Eng. C*, **77**, 4653 (2011) (in Japanese).

35. A. KITAMURA et al., "In-Cell Maintenance by Manipulator Arm with 3D Workspace Information Recreated by Laser Rangefinder," *Nucl. Eng. Des.*, **241**, 2614 (2011).

36. 3Dconnexion Web site: http://www.3dconnexion.com/products/spacenavigator.html (current as of Jan. 6, 2013).

Attachment Design of an Automatic Thrombus Monitoring System Using Multiple Optical Emitters and Detectors for an Extracorporeal Pulsatile Artificial Heart

S. Tsujimura[1] and Y. Sankai[2]

[1] Center for Cybernics Research, University of Tsukuba, Tsukuba, Japan
[2] Faculty of Engineering, Information and Systems, University of Tsukuba, Tsukuba, Japan

Abstract— **Since patients with extracorporeal pulsatile artificial hearts are always exposed to thromboembolic risk, medical staff is forced to regularly conduct visual observation of adherent thrombi inside the artificial heart over the long term. In order to reduce the burden on medical staff and accomplish objective and continuous thrombus monitoring, the purpose of this study was to propose an automatic thrombus monitoring system using multiple optical emitters and detectors for an extracorporeal pulsatile artificial heart, and design its attachment for accurate measurement. The proposed system monitors thrombi by distinguishing a difference in the light absorption and scattering characteristics between the thrombus and the whole blood, on the external surface of the artificial heart without blood contact. To accurately monitor adherent thrombi inside the artificial heart over a wide area, the system needs to firmly attach multiple optical emitters and detectors to the surface of the artificial heart. An attachment including an inner cover and an outer cover was designed. The inner cover where multiple optical emitters and detectors can be arrayed was designed based on the external shape data of an extracorporeal pulsatile artificial heart which were obtained by using a 3D scanner. The outer cover was designed to attach the inner cover to the external surface of the artificial heart. The outer cover connects to the inner cover via spring mechanism, firmly attaching the inner cover to that of the artificial heart by the spring force when the outer cover is closed. The result of an installation test using the prototype attachment showed that the measurement error due to the installation was less than 2% and has little influence on the thrombus monitoring. We conclude that the attachment has the capability to firmly fix the measurement points for accurate monitoring.**

Keywords— **Attachment design, automatic thrombus monitoring system, multiple optical emitters and detectors, extracorporeal pulsatile artificial heart**

I. Introduction

The number of patients who require heart transplantation is increasing yearly. However, the chronic lack of donor hearts greatly restricts the wider implementation of heart transplantation in heart failure patients. As such, the development of artificial hearts has progressed remarkably. There are extracorporeal pulsatile artificial hearts for relatively-short usage as a type of artificial heart. One of serious complications in patients with extracorporeal pulsatile artificial hearts is thromboembolism during the chronic phase [1–3]. The thromboembolism occurs if an adherent thrombus collapses inside the artificial heart and enters the blood stream as thromboemboli (see Figure 1). Therefore it is highly desirable to noninvasively and continuously monitor the adherent thrombus over the long term

At present, to monitor the thrombus, medical staff regularly conducts visual observation of the thrombus on the inside surface of the artificial heart. However, this visual observation not only takes time, but also is discontinuous monitoring and lacks objectivity. Several research groups including ours have reported optical methods and optical measurement systems for noninvasively and continuously detecting thrombus formation or thromboemboli in artificial hearts [4–7]. However, the measurement areas in these studies are limited to the inside of blood circulation tubes connected to the artificial heart and are not the inside surface of the artificial heart.

In the present study, we utilized the knowledge from the above previous studies that thrombus formation or a thromboembolus is detected by a difference in the light absorption and scattering characteristics between the thrombus and the whole blood. The purpose of this study was to propose an automatic thrombus monitoring system using multiple optical emitters and detectors for the detection of adherent thrombi on the inside surface of an extracorporeal pulsatile artificial heart, and design its attachment for accurate measurement.

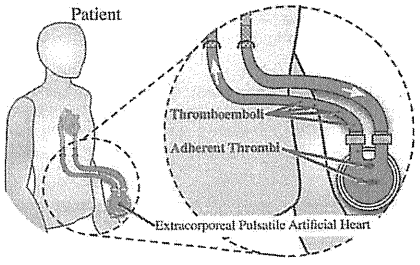

Fig. 1 Adherent thrombi and thromboemboli which induce thromboembolism in the extracorporeal pulsatile artificial heart.

J. Goh (ed.), *The 15th International Conference on Biomedical Engineering*, IFMBE Proceedings 43,
DOI: 10.1007/978-3-319-02913-9_226, © Springer International Publishing Switzerland 2014

II. Materials and Methods

A. Propose of an automatic thrombus monitoring system

In the present study, we target the NIPRO-ventricular assist device (VAD; formerly Toyobo-VAD, NIPRO Corp., Osaka, Japan) [1] as an extracorporeal pulsatile artificial heart. The NIPRO-VAD is a pneumatically-driven artificial heart, being widely used in Japan. For the VAD, an automatic thrombus monitoring system is proposed as shown in Figure 2. The proposed system consists of an optical sensing unit attached around the VAD and monitoring software installed on a personal computer (PC) with Bluetooth radio wave technology. The optical sensing unit has the following four components: (i) multiple optical emitters and detectors for a wide measurement area, (ii) a microcontroller driving the emitters and the detectors and measuring optical intensities from the detectors, (iii) a Bluetooth module for wirelessly transferring the measurement data to the PC, and (iv) an attachment for fixing the other three components around the VAD. In the present, we focus on the attachment and describe the attachment design in the following section.

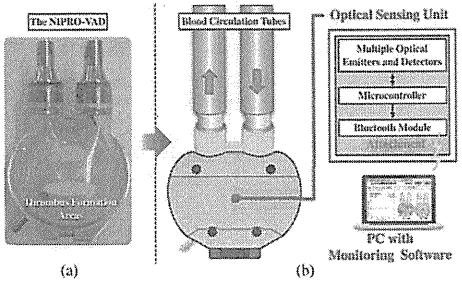

Fig. 2 Configuration of the proposed automatic thrombus monitoring system. (a) Generation areas of adherent thrombi in the NIPRO-VAD, as the monitoring target. (b) The optical sensing unit covers the VAD, wirelessly transmitting the measurement data to the PC.

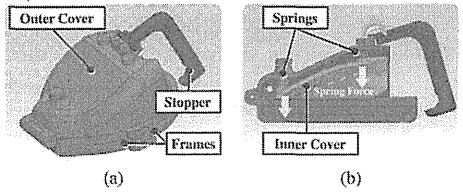

Fig. 3 Design of the attachment. (a) Overall view. (b) Cross-section view.

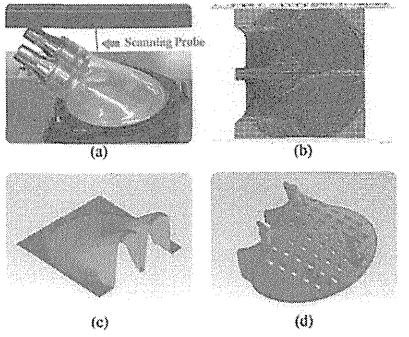

Fig. 4 Design procedure of the inner cover. (a) Scan of the external surface of the NIPRO-VAD by a 3D scanner. (b) The scanned surface data saved as the STL format. (c) The surface data imported into 3D CAD software. (d) Final design by the software.

B. Design of the attachment

In clinical practice, the NIPRO-VAD is put in a special belt bag worn at the waist of the artificial patient. Therefore the size and shape of the attachment must be considered to put the VAD with the attachment in the bag. Furthermore, the attachment must be easily removable for medical treatments (e.g., replacement of the VAD) as needed. To accurately monitor adherent thrombi inside the artificial heart over a wide area, the system needs to firmly fix the multiple optical emitters and detectors to the external surface of the VAD.

The designed attachment consists primarily of an outer cover, a stopper, two frames, spring mechanism using three springs, and an internal cover (see in Figure 3). The outer cover connects to the inner cover via the spring mechanism, firmly attaching the inner cover to the external surface of the VAD by the spring force when the outer cover is closed by the stopper.

The inner cover is expected to incorporate the multiple optical emitters and detectors, and must fit the external surface of the VAD for stable measurement. The inner cover was designed by design procedure as shown in Figure 4. Firstly, the external shape data of the VAD were obtained by a 3D scanner (PIX-30, Roland DG Corp., Shizuoka, Japan), being saved as standard triangulated language (STL) format. Secondly, the STL data was imported to 3D computer-aided design (CAD) software (SolidWorks 2011, Dassault Systèmes SolidWorks Corp., Concord, MA, USA). Finally, the inner cover where multiple optical emitters and detectors can be arrayed was designed as shown in Figure 4(d).

C. Prototype Attachment

Figure 5 shows a prototype of the designed attachment. The parts of the prototype attachment are mainly plastic, being produced by using a 3D printer (Dimension BST 1200, Stratasys Ltd., Minneapolis, MN, USA). These parts are black color to shade the optical detectors from ambient light for accurate measurement. The two plastic frames fitting the center metal ring of the NIPRO-VAD [see Figure 2(a)] are closed by the magnet force of two small neodymium magnets embedded in the frames. At the space between the outer cover and the inner cover, both the microcontroller and the Bluetooth module of the optical sensing unit can be placed. The attachment size is restricted to the minimum necessary for covering the external surface of the VAD. Thus the VAD with the attachment can be put in the belt bag.

D. Installation test using the prototype attachment

In order to evaluate the installation error of the prototype attachment, an installation test using the attachment was performed in a mock circulatory loop that assumed a real operating environment.

The mock circulatory loop was constructed as shown in Figure 6(a). This mock circulatory loop consisted of a reservoir, Tygon tubing, and the NIPRO-VAD with the prototype attachment. The mock circulatory loop was filled with bovine whole blood as the working fluid. The acid-citrate-dextrose solution was previously injected into the blood for anticoagulation. The hematocrit of the blood was adjusted to 40 % by blood draw and injection of saline through the port of the circulatory loop. The beating rate and the stroke volume of the VAD were set to about 60 bpm and 50 ml, respectively.

In the attachment, a photodiode and a phototransistor were incorporated in the inner cover to monitor a generation area of adherent thrombi on the internal surface of the VAD [see Figure 6(b)]. The distance between the photodiode and the phototransistor was 4.5 mm which enabled the light propagation area to include the blood layer of the VAD. If the attachment does not fit the VAD, the output of the phototransistor must change because of the installation error whenever the attachment is removed and attached. The photodiode has the wavelength of 805 nm, which is known as the isosbestic point [8]. Since the optical absorption ratio of hemoglobin equals to the ratio of oxyhemoglobin at the wavelength of 805 nm, the output of the phototransistor is not affected by the oxidization state of the blood during the test. In the initial state, the optical power of the photodiode was adjusted so that the output of the phototransistor was 1.0 V. The output data were measured at 100 Hz sampling frequency by a 16-bit resolution analog-to-digital card [ADA16-32/2(CB)F, CONTEC Co., Ltd., Osaka, Japan], being saved in a PC.

During the test, an installation trial was carried out 10 times. At one time, the average value of the output data for 10 s was recorded 1 minute later after the attachment was removed and attached.

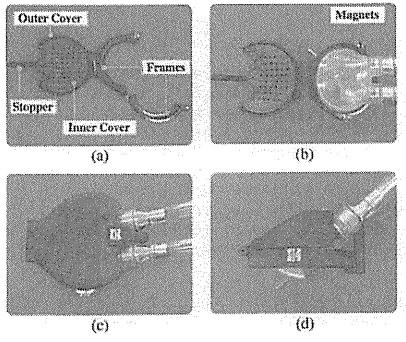

Fig. 5 Appearance of a prototype of the designed attachment. (a) Unattached status. (b) The frames fitting the center metal ring of the NIPRO-VAD. (c) Top view. (d) Side view.

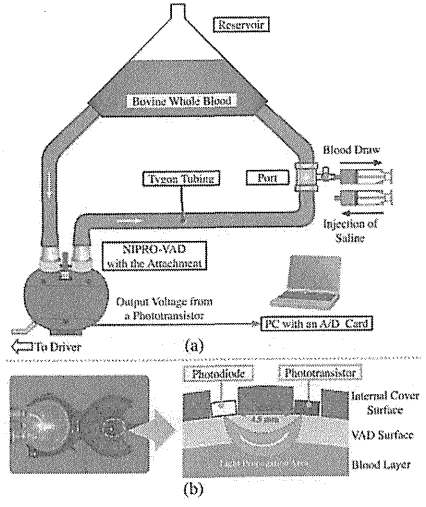

Fig. 6 System configuration of the installation test. (a) Mock circulatory loop filled with bovine whole blood. (b) A photodiode and a phototransistor incorporated in the inner cover.

III. Results

Through the installation test, the average and the standard deviation of the 10 trials were 1.001 V and 0.007 V, respectively. The maximum installation error was less than 2% compared with 1.0 V as the initial value when the average value was 0.987 V. Furthermore, the output of the phototransistor didn't change while the room light was repeatedly turned off and on during the test.

IV. Disscusion

Adherent thrombus formation is a critical issue in the extracorporeal pulsatile artificial heart. A method for monitoring an adherent thrombus is needed in order to ensure safe and effective medical treatment.

In the present study, we proposed an automatic thrombus monitoring system for an extracorporeal pulsatile artificial heart, and designed its attachment for accurate measurement.

To evaluate the installation error of a prototype of the designed attachment, an installation test using the prototype attachment was performed. As a result, the measurement error due to the installation was less than 2%. Generally speaking, the size of the adherent thrombus observed by medical staff is more than several square millimeters at best. Therefore when such an adherent thrombus is generated in the light propagation area on the internal surface of the NIPRO-VAD, the output of the phototransistor is expected to change significantly because the adherent thrombus influences the light propagation. Therefore we suppose that the install error has little influence on thrombus monitoring.

At present, to monitor the adherent thrombus in the extracorporeal pulsatile artificial heart, medical staff is forced to regularly conduct visual observation of adherent thrombi inside the artificial heart over the long term. Moreover, this visual observation is discontinuous monitoring and lacks objectivity. Several research groups have reported optical methods and systems for noninvasively and consciously detecting thrombus formation or thromboemboli in artificial hearts [4–7]. However these studies focused on detecting thrombus formation and thromboembolus on the external surface of blood circulation tubes connected to the artificial heart. Therefore, to the authors' knowledge, this is the first report of an automatic thrombus monitoring system which focuses on detecting an adhere thrombus inside the extracorporeal pulsatile artificial heart on the external surface of the artificial heart. In the present study, we focus on the adherent monitoring system for the NIPRO-VAD. However, the procedure of the attachment design is simple and can be applied to other extracorporeal pulsatile artificial hearts.

V. Conclusions

In the present study, we proposed an automatic thrombus monitoring system, designing its attachment for accurate measurement by using a 3D scanner and 3D CAD software, prototyping the attachment by using a 3D printer. The result of an installation test using the prototype attachment showed that the measurement error due to the installation was less than 2% and has little influence on the thrombus monitoring. Therefore, we conclude that the attachment has the capability to firmly fix the measurement points on the predetermined positions for accurate monitoring.

The further development of the thrombus monitoring system will contribute toward the safety of the patients and the reduction of the burden on medical staff.

Acknowledgment

This study was supported by the "Funding Program for World-Leading Innovative R&D on Science and Technology (FIRST Program)."

References

1. Saito S, Matsumiya G, Sakaguchi T et al. (2009) Fifteen-year experience with Toyobo paracorporeal left ventricular assist system. J Artif Organs 12:27–34
2. Etz C, Welp H, Rothenburger M et al. (2004) Analysis of platelet function during left ventricular support with the Incor and Excor system. Heart Surg Forum 7:E423–E427
3. Samuels LE, Holmes EC, Garwood P, Ferdinand F (2005) Initial experience with the Abiomed AB5000 ventricular assist device system. Ann Thorac Surg 80:309–312
4. Reynolds LO, Mohammad SF, Solen KA, Pantalos GM, Burns GL, Olsen DB (1990) Light scattering detection of microemboli in an extracorporeal LVAD bovine model. ASAIO Trans 36:M518–M521
5. Sankai Y, Tsutsui T, Jikuya T, Shigeta O, Ohta M, Mitsui T (1997) Method of noninvasive and continuous hemolysis/thrombogenesis measurement by laser photometry during artificial heart development. Asaio J 43:M682–M686
6. Solen K, Sukavaneshvar S, Zheng Y et al. (2003) Light-scattering instrument to detect thromboemboli in blood. J Biomed Opt 8:70–79
7. Tsujimura S, Koguchi H, Yamane T, Tsutsui T, Sankai Y (2008) Development of noninvasive thrombus detection system with near-infrared laser and photomultiplier for artificial hearts. Proc. 13th Int Conf on Biomed Eng, Singaproc, 2008, pp 635–638
8. Johnson C, Guy A (1972) Nonionizing electromagnetic wave effect in biological matherials and systems. Proc. IEEE 60:692–718

Author: Shinchi Tsujimura
Institute: Center for Cybernics Research, University of Tsukuba
Street: 1-1-1 Tennoudai
City: Tsukuba
Country: Japan
Email: tujimura@golem.kz.tsukuba.ac.jp

Hindawi Publishing Corporation
Case Reports in Orthopedics
Volume 2013, Article ID 621405, 4 pages
http://dx.doi.org/10.1155/2013/621405

Hindawi

Case Report

A Newly Developed Robot Suit Hybrid Assistive Limb Facilitated Walking Rehabilitation after Spinal Surgery for Thoracic Ossification of the Posterior Longitudinal Ligament: A Case Report

Harutoshi Sakakima,[1] Kosei Ijiri,[2] Fumiyo Matsuda,[1] Hiroyuki Tominaga,[2] Takanori Biwa,[3] Kazunori Yone,[1] and Yoshiyuki Sankai[4]

[1] *Course of Physical Therapy, School of Health Sciences, Faculty of Medicine, Kagoshima University, 8-35-1 Sakuragaoka, Kagoshima 890-8544, Japan*
[2] *Department of Orthopedic Surgery, Faculty of Medicine, Kagoshima University, Japan*
[3] *Fujiyoshi Orthopedic Hospital, Kagoshima, Japan*
[4] *Faculty of Systems and Information Engineering, Center for Cybernics Research, University of Tsukuba, Ibaraki 305-8575, Japan*

Correspondence should be addressed to Harutoshi Sakakima; sakaki@health.nop.kagoshima-u.ac.jp

Received 13 September 2013; Accepted 30 October 2013

Academic Editors: I. Madrazo, G. Onambele-Pearson, and P. Perrini

Most patients with thoracic ossification of the posterior longitudinal ligament (OPLL) exhibit delayed recovery of gait dysfunction after spinal injury. The hybrid assistive limb (HAL) is a new robot suit controlling knee and hip joint motion by detecting very weak bioelectric signals on the surface of the skin. This study is to report the feasibility and benefits of patient-assistive HAL walking rehabilitation for facilitating locomotor function after spinal surgery. The patient was a 60-year-old woman with thoracic OPLL, and her motor and sensory paralyses did not improve after spinal surgery, indicating severe impairment in the paretic legs. The subject underwent 6 HAL sessions per week for 8 weeks, consisting of a standing and sitting exercise and walking on the ground with HAL. Clinical outcomes were evaluated before and after HAL training and 1 year after surgery. The subject improved considerably as a result of HAL training. Subsequently, her walking ability recovered rapidly, and she was able to walk unaided six months after surgery. This case study suggests that HAL training is a feasible and effective option to facilitating locomotor function and the early HAL training with physiotherapy may enhance motor recovery of patients with residual paralysis after surgery.

1. Introduction

Decompression is the primary treatment for patients with compressive myelopathy due to thoracic ossification of the posterior longitudinal ligament (OPLL) and ossification of the ligamentum flavum (OLF), but surgical outcomes vary. Studies of postoperative clinical outcomes of thoracic OPLL indicate that most patients exhibit delayed recovery of motor weakness in the lower limbs and gait dysfunction after surgery [1, 2]. Gait dysfunction is the most important negative surgical outcome, being a clinical deficit of spinal myelopathy [3].

Robotic therapy is becoming increasingly common for gait rehabilitation after stroke or spinal cord injury, using an exoskeleton robotic device (e.g., Lokomat, LOPES exoskeleton robot) or a robotic device with foot-driven plates (e.g., Gait Trainer GT I, Haptic Walker) [4–6]. The robot suit hybrid assistive limb (HAL) is a new robot suit to assist voluntary control of knee and hip joint motion by detecting very weak bioelectric signals on the surface of the skin [7]. The HAL suit is a hybrid control system comprising cybernic voluntary control (CVC) and cybernic autonomous control (CAC) subsystems and has power units and force-pressure sensors in the shoes [8, 9]. The power units consist of angular sensors and actuators on the bilateral hip and knee joints (Figure 1). The HAL suit can support the wearer's motion by adjusting the level and timing of assistance [7]. HAL training, using muscle activity, has the potential to intensify the feedback by evoking by an appropriate motion more strongly than standard robot training [9]. HAL training has been shown to improve gait speed or cadence for chronic stroke and incomplete spinal cord injury [8, 9]. However, no studies have attempted to clarify the feasibility of rehabilitation with HAL for patients with residual paralysis after spinal decompression for thoracic OPLL or OLF.

This case was markedly improved locomotor function by training with HAL, although recovery did not start until 7 weeks after spinal decompression of thoracic OPLL. Therefore, we report a case of patient-assistive HAL walking rehabilitation from an early stage for facilitating locomotor functions for patients with severe residual paralysis.

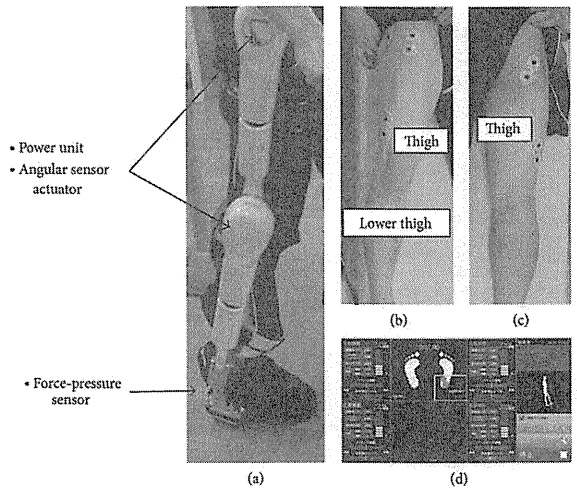

FIGURE 1: Newly-developed wearable robot suit, hybrid assistive limb (HAL). The HAL suit has power units and force-pressure sensors in the shoes. The power units consist of angular sensors and actuators on bilateral hip and knee joints (a). Muscle action potentials are detected through the electrodes on the anterior and posterior surface of the thigh ((b), (c)). Assist levels and force-pressure are shown on a computer monitor (d).

2. Case Presentation

A 60-year-old woman (body mass index: 31.1 kg/m^2) presented with onset of pain and numbness in her right lower limb and gait disturbance. The diagnosis was cervico-thoracic OPLL. After 15 months, her symptoms had gradually progressed, showing motor and sensory paresis of the lower limb and urinary disturbance. Magnetic resonance imaging showed areas of OPLL extending from T2 to T8 and T9/T10 OYL (Figure 2). Because of progressive myelopathy, she underwent posterior decompression surgery two times. However, she showed aggravation of myelopathy after the second surgery, complete motor and sensory paralysis below T4, and urinary retention. She then underwent anterior decompression surgery to remove the OPLL. Active movement of her toes was weak at 1 day after surgery. She underwent physical therapy (PT) with pharmacological and high atmospheric pressure oxygen inhalation therapy. However, her motor and

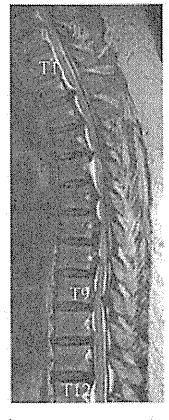

FIGURE 2: T1-weighted magnetic resonance imaging showed areas of OPLL extending from T2 to T8 and T9/T10 OYL.

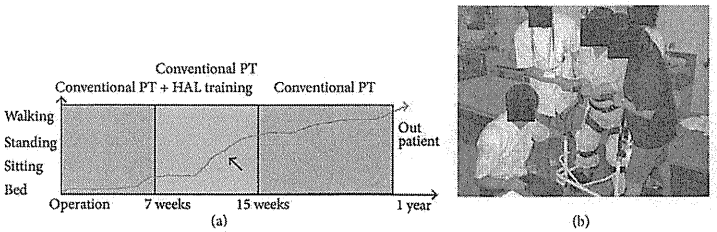

(b)


(c)


(d)

FIGURE 3: Improvement time course of activity of the patient in a schematic view (a). Although she underwent conventional physical therapy (PT), she was still bedridden 7 weeks after surgery. Locomotor functions of the patient improved considerably by intervention of the robot suit hybrid assistive limb (HAL) training. Subsequently, the walking ability recovered rapidly (arrow). When she put on the HAL at baseline, she could stand for only few seconds with assistance from three tree therapists (b). However, she could walk in the parallel bars at 12 weeks after surgery (c) and could walk independently 1 year after surgery (d).

sensory paralyses did not improve. She was still bedridden 7 weeks after surgery and at risk of disuse syndrome. We decided to use HAL in addition to the conventional PT such as muscle strength exercises and range of motion exercises. Before participating in walking exercise using HAL, the subject provided informed consent, and the study was approved by the Ethics Committee of the Kagoshima University Faculty of Medicine.

Clinical assessments were carried out at the initial evaluation (at 7 weeks after final surgery) and 8 weeks and 8 months after HAL intervention (15 weeks and 1 year after surgery, resp., Table 1). After the initial evaluation, the subject underwent 6 HAL sessions of 70 minutes per week for 8 weeks. Sessions consisted of a standing and sitting exercise, and walking on the ground with HAL. Standing and walking training started in parallel bars with HAL. A typical 70-minute HAL training session proceeded as follows: preparation of electrodes, putting on the HAL suit, and computer setup (15 min); HAL training (40 min, including rest time); taking off the HAL suit and electrodes (15 min). Three therapists implemented the training. The HAL suit has a hybrid control system comprising the CVC and CAC. The CVC mode of the HAL suit can support the patient's voluntary motion according to the voluntary muscle activity and the assistive torque provided to each joint [9]. This study used the CVC mode, which allows the operator to adjust the degree of physical support to the patient's comfort and gradually reduce support as training progresses. After the end of HAL intervention, the patient underwent conventional PT without HAL in another hospital, and she was discharged 10 months after surgery.

TABLE 1: Baseline and clinical assessment during follow-up period.

	7 weeks (baseline)	15 weeks (end of HAL)	After 1 year
MMT (U/L)	5/1-2	5/3-4	5/4$^+$-5
JOA score	8	11	13
ASIA classification	C	D	D
ASIA score (lower limbs)	23	34	42
WISCI II	0	8	20
FIM motor score	22	40	83

MMT: Manual muscle testing. JOA: Japan orthopedic association (maximum score: 17). ASIA: American spinal injury association. WISCI: Walking index for spinal cord injury (score range 0 to 20). FIM: Functional independence measure (maximum score: 91).

Locomotor functions of the patient improved considerably by the intervention of HAL training. Subsequently, her walking ability recovered rapidly and she was able to walk independently six months after surgery. Figure 3 shows the improvement time course of activity of the patient in a schematic view. At 15 weeks after surgery, she was able to sit without back support and transfer to a wheelchair independently. She could walk in parallel bars without HAL, although rocking of the knee was observed while standing. At 1 year after surgery, she was able to walk independently with a T-cane.

3. Discussion

This case report describes the feasibility of facilitating locomotor functions with HAL training for patients with residual paralysis after spinal surgery. Matsumoto et al. [10] reported improvement in 36.8% of patients but deterioration in 8.4% after spinal surgery for thoracic OPLL in a retrospective multicenter study of 154 Japanese hospitals. The present patient was operated on 3 times and showed aggravation of her lower limb myelopathy after surgery. Although recovery did not start until 7 weeks after surgery, her locomotor function markedly improved by combining training with HAL, suggesting that HAL training facilitated recovery of locomotor functions. The HAL may facilitate rehabilitation by providing postural support and assisted voluntary muscle activity during ambulation.

HAL is a robotic device with potential rehabilitation applications that are dependent on the physical support it can provide [9]. A patient's recovery of locomotor functions may be due to changes in plasticity of the spinal cord and supraspinal centers. Appropriate sensory inputs, such as maximum weight loading, facilitating proper trunk posture, and hip extension, are essential for maximizing functional recovery [11]. Sensory input evoked HAL-induced motion may affect the central nervous system, resulting in recovery of locomotor functions. Furthermore, the visual feedback of watching a display indicating the center of gravity and range of motion of the lower limbs may also affect the central nervous system. HAL rehabilitation can be implemented safely and effectively for early mobilization and gait training for patients with residual paralysis after spinal surgery.

This study had a clear limitation in that the HAL training was started relatively soon after surgery. However, even if this patient was still in the recovery period, her locomotor function markedly improved by combining training with HAL. HAL training at an early stage may be necessary to prevent disuse syndrome such as muscle weakness in the lower limbs or joint contracture. The subject may also have experienced improved motivation for rehabilitation by HAL training use from an early stage, because she had been bedridden for 7 weeks after surgery. The findings from this case report suggest that HAL training for voluntary control of leg joint motion from an early phase is a safe and effective option for restoring locomotor functions in patients with residual paralysis after spinal surgery.

4. Conclusion

We concluded that for patients of thoracic OPLL, the early HAL training with physiotherapy may enhance motor recovery after surgery. Early mobilization using HAL may be also advocated to prevent post surgery complications, such as contractures and deep vein thrombosis.

Conflict of Interests

The authors have no competing financial interest to declare.

Acknowledgments

This work was supported by Grant no. 23500590 (Harutoshi Sakakima) and Grant no. 23390369 (Kosei Ijiri) from the Japanese Ministry of Culture, Education and Science. This study was supported by the "Funding Program for World-Leading Innovative R&D on Science and Technology (FIRST Program)."

References

[1] M. Takahata, M. Ito, K. Abumi, Y. Kotani, H. Sudo, and A. Minami, "Clinical results and complications of circumferential spinal cord decompression through a single posterior approach for thoracic myelopathy caused by ossification of posterior longitudinal ligament," *Spine*, vol. 33, no. 11, pp. 1199–1208, 2008.

[2] K. Yamada, K. Nagata, K. Sato et al., "Posterior depression by posterior approach for ossification of posterior longitudinal ligament," *Seikeigeka to Saigaigeka*, vol. 57, no. 1, pp. 110–115, 2008 (Japanese).

[3] S. Yu, D. Wu, F. Li, and T. Hou, "Surgical results and prognostic factors for thoracic myelopathy caused by ossification of ligamentum flavum: posterior surgery by laminectomy," *Acta Neurochirurgica*, vol. 155, no. 7, pp. 1169–1177, 2013.

[4] M. Visintin, H. Barbeau, N. Korner-Bitensky, and N. E. Mayo, "A new approach to retrain gait in stroke patients through body weight support and treadmill stimulation," *Stroke*, vol. 29, no. 6, pp. 1122–1128, 1998.

[5] G. Colombo, M. Joerg, R. Schreier, and V. Dietz, "Treadmill training of paraplegic patients using a robotic orthosis," *Journal of Rehabilitation Research and Development*, vol. 37, no. 6, pp. 693–700, 2000.

[6] C. Tefertiller, B. Pharo, N. Evans, and P. Winchester, "Efficacy of rehabilitation robotics for walking training in neurological disorders: a review," *Journal of Rehabilitation Research and Development*, vol. 48, no. 4, pp. 387–416, 2011.

[7] H. Kawamoto and Y. Sankai, "Power assist method based on phase sequence and muscle force condition for HAL," *Advanced Robotics*, vol. 19, no. 7, pp. 717–734, 2005.

[8] S. Maeshima, A. Osawa, D. Nishio et al., "Efficacy of a hybrid assistive limb in post-stroke hemiplegic patients: a preliminary report," *BMC Neurology*, vol. 11, article 116, 2011.

[9] S. Kubota, Y. Nakata, K. Eguchi et al., "Feasibility of rehabilitation training with a newly developed wearable robot for patients with limited mobility," *Archives of Physical Medicine and Rehabilitation*, vol. 94, no. 6, pp. 1080–1087, 2013.

[10] M. Matsumoto, K. Chiba, Y. Toyama et al., "Surgical outcomes and prognostic of ossification of longitudinal ligament in thoracic spine -retorospective multicenter study," *Nihonsekitsuisekizuibyougakai*, vol. 18, no. 1, p. 14, 2007 (Japanese).

[11] H. Barbeau, "Locomotor training in neurorehabilitation: emerging rehabilitation concepts," *Neurorehabilitation and Neural Repair*, vol. 17, no. 1, pp. 3–11, 2003.

2013 IEEE/RSJ International Conference on
Intelligent Robots and Systems (IROS)
November 3-7, 2013. Tokyo, Japan

Development of Noise Resistant Hybrid Capacitive-Resistive Electrodes for Wearable Robotics, Computing and Welfare*

Alexsandr I. Ianov, *Student Member, IEEE*, Hiroaki Kawamoto, *Member, IEEE*
and Yoshiyuki Sankai, *Member, IEEE*

***Abstract*—Myoelectrical signals have many applications in medical, sports, wearable robotics and computing fields. Wet electrodes are widely used to acquire these signals. In contrast, dry contact electrodes and noncontact capacitive coupling electrodes have been developed. However, their use has several limitations. In this research, we developed a hybrid electrode that is capable of both capacitive and resistive recordings by optimizing the sensor input impedance value using a new electrode noise model that contained noise sources. We extend this design so that noise originated during real usage, such as motion artifacts and noise from electric motors is also measured and removed from the sensor output. In experiments, noise analysis and experiments were performed by measuring myoelectrical signals from both upper and lower limbs in realistic situations, including weight lifting, robot arm control, and walking on a treadmill. As the results, we verified that our electrodes were capable of bioelectrical measurements at noise levels comparable to wet electrodes in realistic situations and with high correlation coefficients between both types of sensors.**

I. Introduction

Bioelectrical signals generated by muscle activity, known as myoelectricity, have become an important source of information about movement intention. Myoelectrical signals have been useful for interfacing with physically assistive devices, such as the Robot Suit HAL [1-3], and prosthetic limbs [4-5]. Applications on other areas of human life, such as entertainment industry and virtual reality are also gathering attention [6-7]. However, for such fields, high usability is a requirement alongside high performance.

Traditionally, wet electrodes have been widely used to perform myoelectrical measurements. Because the measurements rely on a passive and resistive electrical contact point, using wet electrodes has major drawbacks such as the requirement for skin preparation and the use of conductive gels [8]. Dry resistive electrodes have been developed to increase sensor performance and usability [9-10]. The dry electrodes rely on active resistive contact with the user's skin surface. Active sensing eliminates the need to use the conductive gels and the problems associated with its use. However, skin preparations such as body hair removal and cleaning may be required because constant electromechanical skin contact is still required for bioelectrical sensing. In order to eliminate this requirement, noncontact electrodes that are capable of achieving capacitive coupling between the electrode lead and the user's skin have been proposed [11-15]. However, ultra-high input impedance is required. Ultra-high impedance input is highly susceptible to any electrostatic noise that originates from the surroundings. Therefore, robust shielding, isolation, and current leakage prevention techniques are mandatory to reduce the noise. Furthermore, complex low noise bootstrapping techniques are necessary to avoid drift due to the bias current from the input. These disadvantages make capacitive electrodes larger, noisier, and more expensive than conventional electrodes.

In order to solve the problems of the previous bioelectrical measurement technologies, we focused in combining the properties of both dry and noncontact electrodes in to a new hybrid resistive-capacitive electrode by optimizing its input impedance so that it is sufficiently high to record bioelectrical signals but low enough to reject external electrostatic noise [16]. However, previous studies consisted of only proof-of-concept basic experiments performed at ideal conditions. Noise from real life situations such as motion artifacts or near high-power devices such as electrical motors are still an issue [13]. In order to solve these problems, the sensor must be designed not only to sensitively measure bioelectrical signals but also to sense and subtract external electrostatic noise from the sensor output.

The aim of this study is to develop a novel hybrid resistive-capacitive electrode using an original sensor based on a circuit model using optimized input impedance for bioelectrical signals while also measuring high frequency noise and removing it from the sensor output. In this study, we focused on a novel extension to our bioelectrical measurement model [16] by actively measuring electrostatic noise and canceling it. This new model allowed us to develop a new electrode design with two inputs, one for electrostatic noise and one for bioelectrical signals, at different input impedance settings which are locally processed using analog circuits. Noise analysis and myoelectricity measurements on lower and upper limbs showed that our electrode maintained a low noise level that was comparable to the noise level maintained by commercially available wet electrodes on both resistive and capacitive modes.

II. Materials and Methods

A. Measurement Principles

Bioelectrical recordings are performed throughout active resistive contact with the skin when the electrodes are capable of electromechanical contact(resistive mode). In the case of poor electromechanical contact conditions, the electrodes measure bioelectrical signals by capacitive coupling with the skin(capacitive mode). The model for our hybrid electrodes contains two built in sensing leads, one for the bioelectrical signals and one for electrostatic noise. The sensor output is given as the difference of potential of both sensing leads as

$$V_{out} = V_{in} - V_{in\_N} \quad (1)$$

where V_{out} is the sensor output, V_{in} is the bioelectrical signal with noise and V_{in_N} is noise originated from motion artifacts or pulses from nearby electrical devices. Figure 1 shows the equivalent circuit when the electrodes are in use. This model also includes noise from capacitive sources as

$$V_{IN} = \frac{R_c}{Z_{nc}}V_{nc} + \frac{R_c}{Z_{nsei}}V_{nsei} + \frac{R_c}{Z_{sei}}V_{BES} \quad (2)$$

where V_{BES} is the bioelectrical signal voltage, V_{nsei} is the total noise source voltage at the skin-electrode surface, V_{nc} is the total noise source voltage on the electrode board, Z_{sei} is the skin-electrode interface impedance, R_c is the electrode input impedance, i.e., the input impedance of the bioelectrical sensing lead, Z_{nsei} is the noise input impedance at the skin-electrode interface, and Z_{nc} is the noise input impedance on the electrode board. This noise can be significant if the electrodes are in capacitive mode. However it can be minimized when the sensor input impedance is optimal. Based on our previous studies [16], we define the input impedance optimal when it is just large enough to allow the sensor electrode to capacitively sense bioelectrical signals. With these settings the sensor input impedance is low enough to reject low frequency capacitive noise signals from the environment. Optimal input impedance is calculated using

$$R_c = \frac{V_{IN}}{V_{BES}} \cdot \frac{d}{\varepsilon_r \varepsilon_0 A 2\pi f} \quad (3)$$

where ε_0 is the dielectric constant in vacuum, ε_r is the relative dielectric constant to the material, A is the electrode lead sensing area nearest to the skin, f is the frequency of the target signal and d is the distance between the skin and the electrode lead.

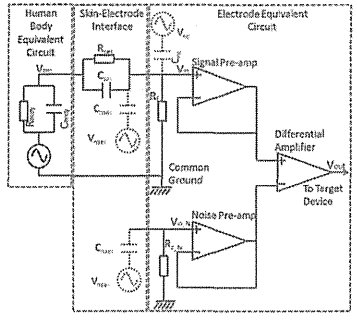

Figure 1. Electrode equivalent circuit

Similar equations are used when calculating the input impedance R_{c_N} of the electrostatic noise electrode lead, but in this case, designing the lead so it can sense only high frequency noise signals over bioelectrical and low frequency noise signals.

B. Developed Hardware and Noise Evaluation

Based on the proposed electrode model and assuming a maximum 3 mm distance between the electrode and the skin, a circular electrode lead with 38mm diameter and signal input impedance of 1 TΩ was developed. Furthermore, in similar fashion the noise electrode lead is designed. Under these conditions a 1 mm thick ring shaped electrode lead with outer radius of 40 mm is designed. Noise input impedance R_{c_N} is also set to 1 MΩ, so that only noise signals with frequency above the myoelectrical frequency spectrum are measured. In resistive contact mode the area of the leads has little effect on the input impedance and low input impedance contact are enough to measure bioelectrical signal. Because of that the noise sensing lead is electrically isolated using a thin layer of plastic coating. Without the coating, in resistive contact mode, very similar bioelectrical signals would be collected by both the bioelectrical and noise sensing leads, canceling each other during the differential preamplifier stage at the electrode. A High Pass Filter circuit is also implemented by using traditional circuits in order to eliminate undesirable offset voltages that can appear due to the difference in potential between both electrode sensing leads. Furthermore, back-to-back diodes are also attached to the leads in order to reduce the effects from input bias current.

In order to further increase sensor robustness, shielding was implemented as shown in Figure 2 by making using of inner layers of the sensor printed circuit board, in which the electronic components as well as most of the circuit pattern is located in the component layer and the sensing leads in the solder layer. The assembled electrode is shown in Figure 3.

The developed electrode data recording and evaluation system is shown in Figure 2, and it includes three stages. In the first stage, a second instrumentation amplifier receives analog

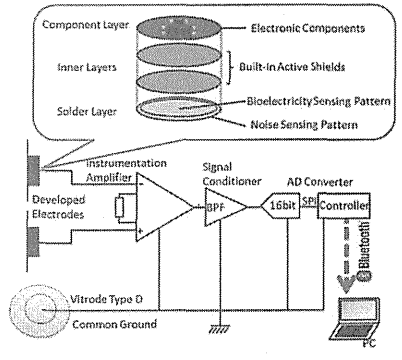

Figure 2. Measurement system diagram

* This study was supported by the "Center for Cybernics Research (CCR) - World Leading Human-Assistive Technology Supporting a Long-Lived and Healthy Society"' granted the "Funding Program for World-Leading Innovative R&D on Science and Technology (FIRST Program)," initiated by the Council for Science and Technology Policy (CSTP).

All the authors are with Cybernics Center, System and Information Engineering, University of Tsukuba, Tsukuba, Ibaraki, 305-8573, Japan (e-mail: ianov@golem.kz.tsukuba.ac.jp; kawamoto@golem.tsukuba.ac.jp; sankai@golem.tsukuba.ac.jp).

978-1-4673-6357-0/13/$31.00 ©2013 IEEE

signals from two electrodes and outputs the amplified difference between them. The second stage is responsible for conditioning the signal for the AD converter. The final stage involved a 16-bit AD converter connected via an SPI channel to a microcontroller. Signal sampling was performed at 1 kHz. Data was transferred from the controller to a laptop computer via a Bluetooth connection. This system is compatible with the hybrid electrodes and the commercially available Vitrode(Nihonkohden, Japan) wet electrodes for simultaneous comparative recordings. The common ground was connected to a clean exposed body area of the user via a stainless steel plate. Each sensor was connected to the system using a 1 meter long cable. Noise frequency spectrum measurement experiments were performed for both resistive and capacitive modes using this system by placing two electrodes face to face on differential input.

C. Upper Limb Myoelectrical Measurement

Lifting objects and moving the arms are important actions when using wearable robotic devices [1-2]. In this study we evaluate the performance of our enhanced hybrid electrodes through a two-part experiment. First part is defined by measuring myoelectrical signals when lifting up and letting down various weights and second part is defined by performing robot arm control using myoelectrical signals.

For the first part of the experiment, myoelectrical signal measurements are performed under various loads. The participant leaves his arm at rest for 5 seconds, slowly starts lifting the load for 5 seconds and then slowly let the load down for another 5 seconds until the arm returns to rest position for the final 5 seconds. Loads of 2.5 kg, 5.0 kg, 7.5 kg and 10 kg were used in this part of the experiment. Simultaneous measurements on both resistive and capacitive mode as well as using standard Vitrode wet electrodes were performed. For both experiments the hybrid electrodes were attached to the biceps of the participant as shown in Figure 4. Methods for attaching the Vitrode wet electrodes and the developed hybrid electrode in both resistive and capacitive modes are shown in Figure 5. The ground electrode was attached to the abdomen of the participant. Electrodes in capacitive mode were separated from the skin through a 1mm cotton shirt. Correlation coefficients between data collected from wet electrodes and hybrid electrodes in resistive and capacitive modes are calculated using Pearson's calculation method.

The second part of the experiment verifies the operation of the hybrid electrodes near electrical appliances by performing simple robot arm control experiment. While leaving the arm at rest, the robotic arm(Jaco by Kinova, Canada) also stayed at a resting position. By lifting the arm in to a 45-degree position, the myoelectrical signals from the biceps switch on the robotic arm, also rotating it 45-degree. Each movement was repeated two times for 10 seconds. The participant's arm was in contact with the robotic arm through the entire experiment. Electrodes were placed in capacitive mode over the arm similarly to the previous weight lifting experiment. Only capacitive mode was measured as it was the weakest to noise and the high correlation coefficient with wet electrodes was confirmed using the results from the first part of the experiment.

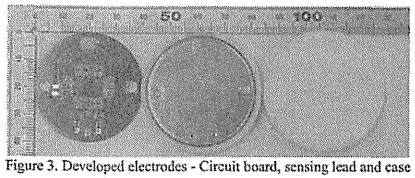

Figure 3. Developed electrodes - Circuit board, sensing lead and case

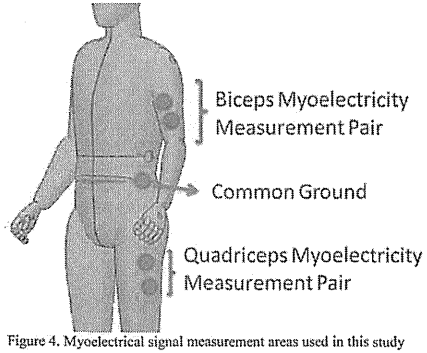

Figure 4. Myoelectrical signal measurement areas used in this study

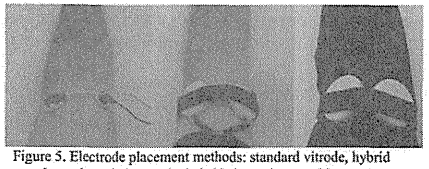
Figure 5. Electrode placement methods: standard vitrode, hybrid electrode resistive mode, hybrid electrode capacitive mode

D. Lower Limb Myoelectrical Measurement

Measurement of myoelectrical signals while walking is a fundamental procedure in lower limb to evaluate walking ability accurately in rehabilitation treatments [3]. In this study we evaluate the performance of our enhanced hybrid electrodes during walking by measuring myoelectrical signals from the quadriceps when the participant walks on a treadmill. The participant walks at a constant speed of 1.2 m/s on a treadmill for a period of 20 seconds. The hybrid electrodes were attached to the quadriceps of the participant as shown in Figure 4. The ground electrode was attached to the abdomen of the participant. Simultaneous measurements on both resistive and capacitive mode were performed. Electrodes in capacitive mode were separated from the skin through a 2.2 mm jeans pants. The correlation coefficient between data sets acquired from both resistive and capacitive modes was calculated.

III. Results

A. Noise Evaluation Results

The noise spectrum in the 1-500 Hz band is shown in Figure 6. The results show that the maximum noise is of 11 $\mu V/Hz^{1/2}$, which happens in capacitive modes at lower frequencies. As myoelectrical signals are in the order of 100-1000 μV and commonly used signals oscillate in the 30-500 Hz band [17], the results show that our enhanced hybrid electrodes are reliable enough for myoelectrical measurements.

B. Upper Lim Myoelectrical Measurement

The recorded experiment data for the bioelectrical signal measurement under variable load part of the experiment is shown in Figure 7. From the results the correlation coefficient between resistive mode and conventional wet electrode mode was of 0.98. The correlation coefficient between capacitive mode and wet electrode was of 0.92. It is important to notice that even though there was constant movement during the period 5-15 s, no motion artifacts were observed in any of the trials with any load. The relatively high myoelectrical signal output observed during the seconds 5 to 7 in all the data sets is the due to the extra power required to surpass the inertia of lifting the load from complete rest.

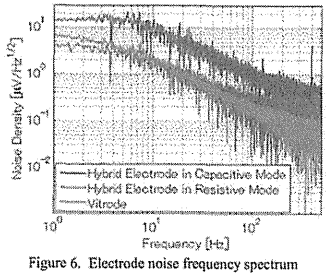

Figure 6. Electrode noise frequency spectrum

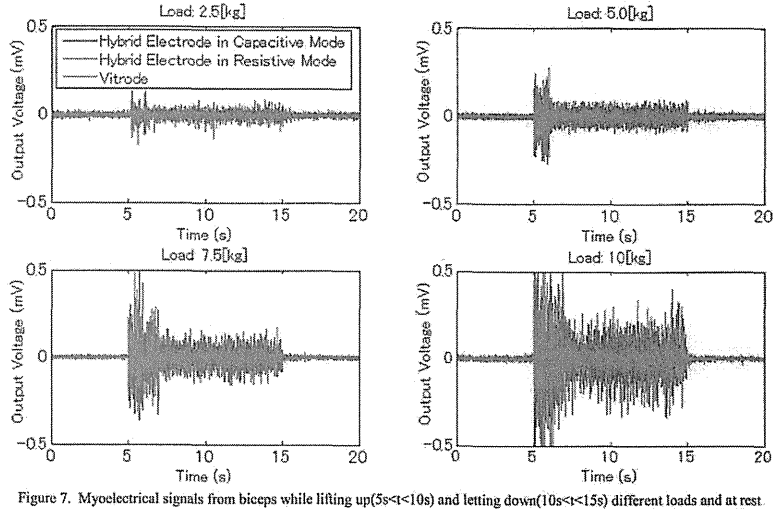

Figure 7. Myoelectrical signals from biceps while lifting up(5s<t<10s) and letting down(10s<t<15s) different loads and at rest

The high correlation coefficient between the hybrid electrode in capacitive mode and wet electrodes suggested that we could use the hybrid electrode for the robot control. Therefore the second part of the experiment was performed using only the hybrid electrode in capacitive mode. The recorded experiment data for the robot arm control experiment is shown in Figure 8. The arm weight was enough to stimulate the biceps and create a signal strong enough to be used as in a simple trigger algorithm. Moreover, the presence of an electrical motor near the electrodes did not interfere with its functionality and no noise was observed.

C. Lower Limb Myoelectrical Measurement

The recorded experiment data for the treadmill walking experiment is shown in Figure 9. The results showed constant myoelectrical activity in the quadriceps suggesting continuous load. In particular, during the walking process, the load is the biggest when there is contact of the leg with the floor. From the results we also can observe that the myoelectrical data collected by the enhanced hybrid electrode in both resistive and capacitive mode is mostly overlapping, with a calculated correlation coefficient of 0.76. No visible motion artifacts from leg movements nor electrostatic noise from the treadmill were observed.

IV. Discussion

One of the key aspects and the breakthrough point of this paper is the implementation of the novel dual signal lead system with a differential preamplifier unit built in the electrode. Comparing to previous studies from other groups [12-15] as well as our own [16], this breakthrough point is better design choice than applying an analog or digital Low Pass Filter during signal conditioning because it removes a

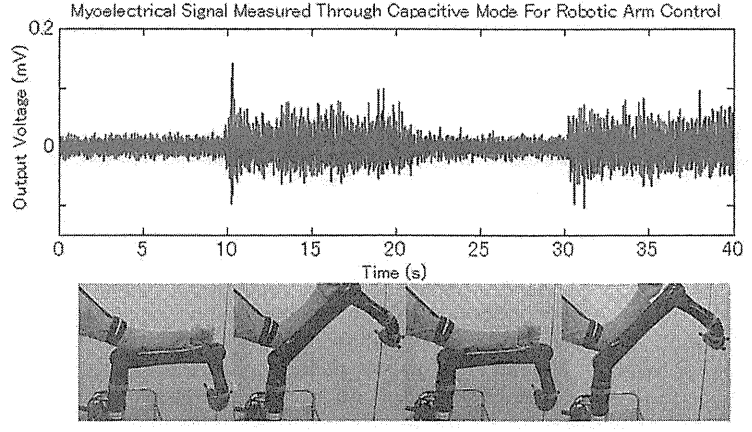

Figure 8. Robot arm movement control experiment using biceps myoelectrical signal measurement

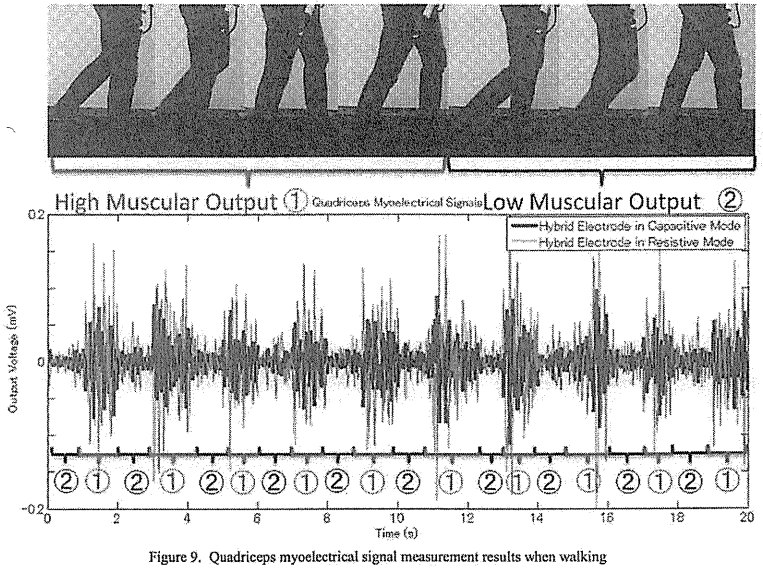

Figure 9. Quadriceps myoelectrical signal measurement results when walking

significant amount of noise before the electrical signal enters our system, avoiding problems caused by the limits on operational amplifiers power supply as well as signal distortion and delays from the filters.

The comparative experiments between our electrodes in both resistive and capacitive mode and standard wet electrodes have shown that our electrodes were capable of measuring myoelectrical signals under conditions simulating real world environments. Measurements performed under the presence of movement and active electromechanical devices nearby matched expected clear recordings that match known phenomena. Our noise frequency analysis shows that our hybrid electrodes have a noise level below 11 $\mu V/Hz^{1/2}$, performing at comparable levels to commercially available electrodes as well as other studies [15]. Furthermore the comparison experiment with commercial electrodes results from Figure 7 and the high correlation coefficient validate the effectiveness of our electrodes.

The single board design which integrates the circuitry, shielding and sensing leads in a single printed circuit board allowed us to make a sensor with 4 mm thickness, which is less than half systems developed in other studies [12-16]. With further miniaturization of electronic components and the use of flexible printed circuit boards, more user friendly sensors can be developed for wearable computing and robotic applications.

In this paper, we used a single conventional electrode made of stainless steel in order to create a robust ground between the user and the electronic system. In order to maximize the usability of the system, we suggest that while designing a wearable robotics or computing system, ground connection should be guaranteed by developing a mechanism in which the user is always in contact with a conductive grounded area of the system.

Myoelectrical signals are used extensively on rehabilitation both as a diagnosis, evaluation tool and as a method for interfacing with assistive devices. Rehabilitation in particular is a medical treatment where user enthusiasm is important, and one of the key factors in maintain enthusiasm is keeping the treatment as accessible as possible, including having an intuitive user interface. The hybrid electrodes developed in this paper using the extended electrode and noise model from Figure 2 are prototype sensors that are capable of measuring bioelectrical signals, regardless of skin contact conditions from both upper and lower limbs while performing movements near electromechanical equipments. This breakthrough is a step towards the prolonged monitoring of bioelectrical signals in a clinical and home environments necessary in rehabilitation treatments. Features such as being able to register myoelectrical signals over clothing, quick sensor placement and being able to using sensors for very long periods of time without signal degradation from sweat and conductive substrate degradation greatly contribute to the increase of usability. Evaluation of the effects that the increased usability have on the total treatment through clinical trials is necessary. Furthermore evaluation of reliability and wearability over long periods of time, such as an entire day or week, is also critical for future medical use as well as for sports and entertainment applications.

V. Conclusion

In this study, we developed a novel hybrid resistive-capacitive electrode using an original sensor based on an model using optimized input impedance for bioelectrical signals while also measuring high frequency noise and removing it from the sensor output. Noise analysis and myoelectricity measurements on lower and upper limbs showed that our electrode maintained a low noise characteristic and bioelectrical sensing performance that was comparable to commercially available wet electrodes.

In future studies, we intend to further increase the accuracy of our electrode model and expand the design to specific applications such as exoskeleton control and virtual reality in the fields of rehabilitation, sports and entertainment. Our sensors help increase the usability and reliability of bioelectrical interfaces and promote the popularization of medical and wearable devices in daily life.

References

[1] T. Hayashi, H. Kawamoto and Y. Sankai, "Control Method of RobotSuit HAL working as Operator's Muscle using Biological and Dynamical Information", Proc. of IEEE/RSJ International Conference on Intelligent Robots and Systems (IROS 2005), pp.3455-3460, 2005

[2] H. Kawamoto and Y. Sankai, "Power assist method based on Phase Sequence and muscle force condition for HAL", Advanced Robotics,vol.19, no.7, pp.717-734, 2005

[3] K. Suzuki, G. Mito, H. Kawamoto, Y. Hasegawa and Y. Sankai, "Intention-Based Walking Support for Paraplegia Patients with RobotSuit HAL, Advanced Robotics", Vol.21, No.12, pp.1441-1469, 2007

[4] Saridis, George N.; Gootee, Thomas P.; , "EMG Pattern Analysis and Classification for a Prosthetic Arm," Biomedical Engineering, IEEE Transactions on , vol.BME-29, no.6, pp.403-412, June 1982

[5] Au, S.K.; Bonato, P.; Herr, H.; , "An EMG-position controlled system for an active ankle-foot prosthesis: an initial experimental study," Rehabilitation Robotics, 2005. ICORR 2005. 9th International Conference on , vol., no., pp. 375- 379, 28 June-1 July, 2005

[6] X. Zhang, X. Chen, W. Wang, J. Yang, V. Lantz, and K. Wang, "Hand gesture recognition and virtual game control based on 3D accelerometer and EMG sensors," Proceedings of the 14th international conference on Intelligent user interfaces (IUI '09), pp. 401-406, 2009

[7] G.M.Lyons, P. Sharma,M. Baker ,S. O"Malley,A. Shanahan, "A computer game-based EMG biofeedback system for muscle rehabilitation," Engineering in Medicine and Biology Society, Proceedings of the 25th Annual International Conference of the IEEE , vol.2, pp.1625-1628, Sept. 2003

[8] J.R. Wolpaw,N. Birbaumer,W.J. Heetderks,D.J. McFarland,P.H. Peckham,G. Schalk, E. Donchin, L.A. Quatrano, C.J. Robinson,T.M. Vaughan, "Brain-computer interface technology: a review of the first international meeting," IEEE Transactions on Rehabilitation Engineering,Vol.8, No.2, pp.164-173, 2000

[9] T.J. Sullivan, S.R. Deiss, T.P. Jung and G. Cauwenberghs: "A brain-machine interface using dry-contact, low-noise EEG sensors", Proc. IEEE Int. Symp. Circuits and Systems, pp.1986-1989, 2008

[10] G. Gargiulo, R. A. Calvo, P. Bifulco, M. Cesarelli, C. Jin, A. Mohamed, A.V. Schaik: "A new EEG recording system for passive dry electrodes", Clinical Neurophysiology, Vol. 121, No. 5, pp.686-693, 2010

[11] C.J. Harland, T.D. Clark and R.J. Prance: "Electric potential probes-new directions in the remote sensing of the human body", Measurement Science and Technology, Vol.2, pp.163-169, 2002

[12] Y.M. Chi, G. Cauwenberghs: "Micropower non-contact EEG electrode with active common-mode noise suppression and input capacitance cancellation," Engineering in Medicine and Biology Society, pp.4218-4221, 2009

[13] Y.M. Chi, T.P. Jung, G. Cauwenberghs: "Dry-Contact and Noncontact Biopotential Electrodes: Methodological Review", IEEE Reviews in Biomedical Engineering, Vol.3, pp.106-119, 2010

[14] J. Harland, T.D. Clark and R.J.Prance:"Electrical potential probes - new directions in the remote sensing of the human body", Measurement Science and Technology, Vol.13, pp.163-169, 2002

[15] A. Lopez and P. C. Richardson: "Capacitive electrocardiographic and bioelectric electrodes", IEEE Transactions on Biomedical Engineering, Vol.16, pp.299-300, 1969

[16] A. I. Ianov, H. Kawamoto, Y. Sankai, "Development of Hybrid Resistive-Capacitive Electrodes for Electroencephalogram and Electrooculogram", IEEJ Transactions of Sensors and Micromachines, Vol. 133, No. 3, 2012

[17] R. E. Gander, B. S. Hutchins, "Power Spectral density of the surface myoelectric signal of the biceps branchii as a function of static load," Electromyography and clinical neurophysiology, Vol. 25, pp. 469-478, 1985

日本機械学会論文集（C編）
79巻804号（2013-8）

原著論文 No. 2012-JCR-0585

簡便な下肢の動脈硬化スクリーニング指標計測装置の開発*

白石 直人*1，山海 嘉之*2

Development of Easy Measurement Device for Screening of Arterial Sclerosis of Lower Limbs

Naoto SHIRAISHI*1 and Yoshiyuki SANKAI

*1 Graduate School of Systems and Information Engineering, University of Tsukuba
Tennodai 1-1-1, Tsukuba, Ibaraki, 305-8573 Japan

In order to prevent and treat arterial sclerosis, a quantitative measurement method is required. The measurement results in daily environment give important information for diagnosis and treatment. In medical institutions, pulse wave velocity (PWV) is used for screening of arterial sclerosis. However, a measurement device for daily environment was yet to be developed. Therefore, the purpose of this research is to develop an easy to use device for PWV measurement in order to perform the screening index of arterial sclerosis for daily use, and to confirm a relationship between PWV that measured with our device and the existing index for screening. We proposed using only an electrocardiogram (ECG) and a photoplethysmogram (PPTG) for the PWV measurement in order to develop an easy to use device. And the device used wireless communication in order to be the least restraintful as possible. We carried out two experiments with the device. An experiment is to confirm the measurement accuracy. Another is to confirm the relationship between the PWV and the existing index. As a result of the experiment of the measurement accuracy on 8 subjects, the average of the coefficient of variation was 2.34%. And result of the experiment of the relationship on 28 subjects showed a significant correlation ($r=0.707$, $p<0.001$) between the PWV and existing index for screening. Hence, we developed the easy to use and non-restraint device and the device was able to measure the PWV with high accuracy, conformed by the high correlation with existing index.

Key Words: Medical and Welfare Assistance, Measurement, Signal Processing, Pules Wave Velocity, Arterial Sclerosis

1. 緒　言

心疾患・脳血管疾患は寝たきりや死亡の原因であり，これらの疾患による死者数は世界で年間1700万人を超える[1]．心疾患・脳血管疾患の主な危険因子は動脈硬化である．動脈硬化の予防や治療において，動脈硬化の状態を把握することが重要であり，そのために動脈の硬さを定量的に計測することが必要となる．動脈の硬さの定量的な指標として普及しているものに脈波伝播速度（PWV: Pulse Wave Velocity）がある[2-4]．PWVを用いた具体的な指標には，心臓足首血管指数(CAVI: Cardio Ankle Vascular Index）や上腕足首脈波伝播速度（baPWV: brachium-ankle Pulse Wave Velocity）等がある[5]．これらの指標は，動脈硬化の中でも患者数の多い閉塞性動脈硬化症がよく生じる下肢の動脈硬化を反映するものであり，専用の装置を用いて医療機関で計測されている．この医療機関での計測に加えて，家庭や職場等で日常的に指標の計測ができれば，動脈硬化の継続的な変化が記録可能となり，記録した情報を診断・治療の参考情報として活用できるようになる．

しかし，医療機関で用いられている計測装置は日常的な利用が困難である．医療機関の装置による計測では，チューブやケーブルで接続されたセンサプローブと大きな装置本体を身体に取り付ける必要がある．そのため利用者が拘束され一人で計測することができず，計測に手間がかかる．したがって，日常的な指標の計測のためには非拘束で簡便に利用できる装置が必要となる．

* 原稿受付　2012年8月28日
*1 正員，筑波大学大学院　システム情報工学研究科（〒305-8573　茨城県つくば市天王台1-1-1）
*2 正員，筑波大学大学院　システム情報工学系
E-mail: shiraishi@golem.kz.tsukuba.ac.jp

従来の装置では，脈波の計測に空気容積脈波を用いているため，コンプレッサ等が必要となり小型化やチューブレス化ができない．したがって，非拘束で簡便な装置の実現には，空気容積脈波を用いない手法が必要である．そこで，心電図と光電脈波を用いたPWVの計測手法が有効であると考えられる．心電図や光電脈波の計測装置は電子回路のみで構成可能なため，小型の機器が実現できる．心電図と光電脈波を用いたPWV計測の基礎的な手法は先行研究によって提案されており，再現性よく計測できることや手先や足先等いくつかの部位でPWVを計測できることが示されている[6-8]．しかし，心電図と光電脈波を用いたPWVが動脈硬化とどの程度対応するのかは検証されていない．また，心電図と光電脈波を用いたPWVの計測手法で日常的な利用を想定した装置を構築できるかは，実際の利用を考慮した装置を開発して評価することが必要であると考えられるが，先行研究では心電図と光電脈波の計測は実験用の計測装置で行われている．

そこで，本研究では日常的な動脈硬化スクリーニング指標の計測を実現するために，センサが取り付け易く非拘束で計測できる簡便な装置を開発すること，ならびに，開発した装置によって計測した下肢に関する動脈硬化のスクリーニング指標が既存の指標と同様に動脈硬化に関連する動脈壁の硬さ対応することを検証することを目的とする．

2. 心電図と光電脈波を用いた脈波伝播速度計測装置の開発

2・1 心電図と光電脈を用いた脈波伝播速度計測方法

脈波は，心臓が血液を拍出することによって生じ，心臓を起点に末梢へ向かって動脈内を伝播する．PWVは、動脈硬化のスクリーニング検査項目であり，動脈壁の硬さを反映する指標として知られている[9-10]．PWVは，伝播距離を伝播時間で割ることで算出される．伝播時間は，脈波を2カ所で計測して求める．このような原理で計測されるため，PWVの計測結果は，脈波の計測部位および伝播時間と伝播距離の算出方法の影響を受ける．本研究における脈波の計測部位および，伝播時間と伝播距離の算出方法を以下に述べる．

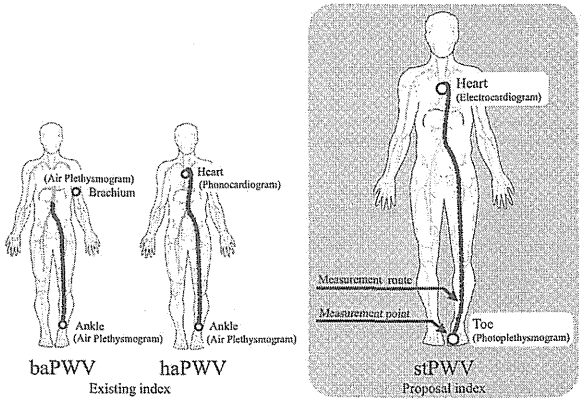

Fig. 1 Measurement points and routes of PWV

脈波の計測部位によって計測対象の動脈が決まる．そのため，硬さを計測する動脈に応じて脈波の計測部位が選択される．これは，基本的に脈波を計測した2カ所の間についてのPWVが得られるためである．実際には，医療機関で用いられているhaPWV（heart-ankle Pulse wave velocity）やbaPWVは，閉塞性動脈硬化症の生じやすい下肢の動脈を含むように脈波の計測部位が選択されている．これらの計測対象の動脈を図1に示す．脈波は心

音図や心電図で代用されることがあり，haPWV では心音が用いられている．なお，haPWV は CAVI の算出に用いられている．そこで，本研究においても下肢の動脈を含む経路を計測対象とする．

下肢の動脈を含んだ経路を簡便に計測できる装置の実現のために，心電図と光電脈波を用いた PWV 計測方法を採用する．光電脈波の計測部位は，足の指先（母指の底面）とした．心電図は，心臓と大動脈のつなぎ目である大動脈基部の脈波の代替とした．これにより，計測対象の動脈は心臓から足の指先となり，下肢の動脈を含んだ経路となる．なお，本研究で計測する PWV は，脈波の計測位置等から stPWV（Sinoatrial node-toe Pulse Wave Velocity）と呼ぶこととする．図 1 のように，stPWV の経路は haPWV の経路とほぼ同様であり，haPWV の経路に足首から足指までの経路を加えたものが stPWV の経路である．

次に心電図と光電脈波による伝播時間の具体的な計測方法について述べる．本研究では，心電図の R 波の最大値を起点とし、脈波の立ち上がり開始点を終点とする時間を伝播時間として定義する．図 2 にこの定義による脈波伝播時間（PTT: Pulse Transit Time）の計測例を示す．図 2 において，黒の実線が心電図（ECG: Electrocardiogram）、灰色の実線が光電脈波（PTG: plethysmogram）である．点線はそれぞれ，心電図の R 波（0.8 s 付近）と脈波の立ち上がり開始点（1 s 付近）に対応する時刻である．一般的に PWV の伝播時間は 2 つの脈波の時間差で定義され，時間差を求めるために脈波の特徴点が決められている．特徴点には波形の立ち上がり開始点が採用されている．立ち上がりの開始点は波形処理方法によりいくつかの決定方法が検討されている[11]．脈波同士で時間差を算出する一般的な場合には，伝播時間を計測するために 2 つの脈波に対して同じ特徴点が用いられる．本研究の stPWV では，大動脈基部での脈波の特徴点を心電図の R 波で代替したため，末梢側の脈波の特徴点を左心室の収縮と関連する点にする必要がある．脈波の最小値は，左心室の収縮により大動脈に血液の拍出が開始された時に生成される点であるため、この点を特徴点として採用した．

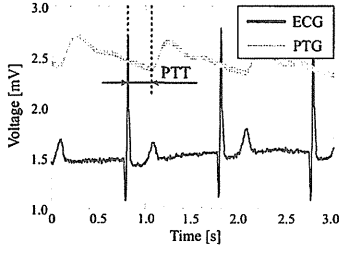

Fig. 2 Pulse transit time (PTT) measured by electrocardiogram (ECG) and plethysmogram (PTG)

最後に脈波の計測部位に対応する伝播距離の算出方法について述べる．本研究では，式（1）に示す身長を用いた推定式により，伝播距離を算出する．ここで，L は伝播距離，H は身長である．

$$L = 0.8129\,H + 47.328 \text{ [cm]} \quad (1)$$

脈波が伝播した動脈の長さを簡便に計測することは困難である．そのため，baPWV や CAVI 等の計測機器では身長を用いて伝播距離が算出されている．式（1）は，baPWV 計測に用いられている伝播距離の推定式[12]をもとに定義した．baPWV 計測で用いられている推定式からは心臓から足首までの伝播距離が得られるため，本研究では足首から足の親指先までの伝播距離を 35[cm]として baPWV 計測で用いられている推定式に加算することで伝播距離を定義した．足首から足の親指先までの伝播距離は，足長[13]と足首から踵までの長さから推定した．

2・2 計測装置の構成

stPWV を計測するための装置を製作した．stPWV 計測装置の構成を図 3 に示す．本装置は，心電図と光電脈波を計測するセンサデバイスと計測した情報を処理して表示するデータ処理表示部で構成した．センサデバイスとデータ処理表示部は無線接続とし，センサデバイス内は有線接続とした．

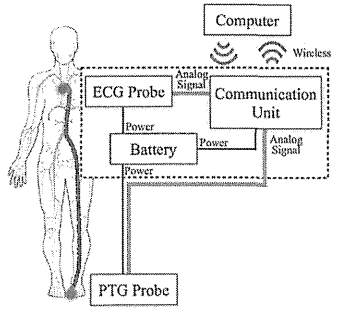

Fig. 3 The system configuration diagram

簡便化のため，センサデバイスの操作部分は電源スイッチのみである．計測は，無線通信を介した制御により自動で行われる．計測開始に必要な操作は，ソフトウェアの開始ボタンの押下のみである．センサデバイスは小型であり，計測データが無線通信で伝送されるため，被計測者を拘束しない．センサデバイスの取り付けは被計測者自身で可能である．

データ処理表示部は，パーソナルコンピュータ（PC）と計測ソフトウェアで構成される．PC は，Windows7 SP1，Java Runtime Environment 1.6 がインストールされているものとする．

本装置は，足の指に脈波プローブを取り付け，左胸部に心電図センサを当てて使用する．計測は，十分な安静の後，プローブ類を取り付け，仰向けの姿勢（仰臥位）で行う．

次項にセンサデバイスとデータ処理表示部の計測ソフトウェアの詳細について述べる．

2・2・1 センサデバイス

製作したセンサデバイスの写真を図 4 に示す．センサデバイスは，図 3 の破線内の部分に相当する通信ユニット兼心電図プローブ（96×60×21 mm）と脈波プローブ（21×17×9 mm）で構成した．脈波プローブは通信ユニットに有線接続されており，通信ユニットからの電力供給とプローブからの計測信号の伝送が行われる．有線接続のため，プローブ側に電源や通信機能が必要なく小型化でき，アナログ信号での伝送を採用することで計測信号を遅延なく伝送可能であり，stPWV 計測のために必要な心電図と脈波信号の同期記録が容易に可能である．

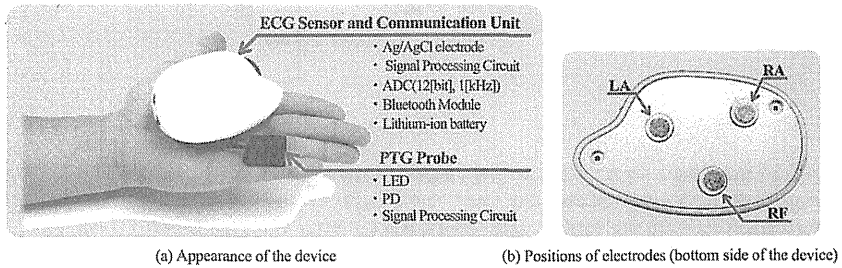

(a) Appearance of the device (b) Positions of electrodes (bottom side of the device)

Fig. 4 The sensor device

通信ユニットは，心電図と脈波の A/D（アナログ/デジタル）変換と無線通信機能を持つ．A/D 変換と通信の制御には，小型化のために 8 mm 角のマイクロコントローラ（dsPIC30F3013，Microchip Technology Inc.）を用いた．無線通信の方式には，汎用性が高く，十分な通信距離と通信速度を確保できる Bluetooth を採用した．Bluetooth

通信用のデバイスとして，シリアル通信が可能なモジュール（KC22，KC wirefree）を用いた．電源には，Li-ion バッテリ（3.7 V，1000 mAh）を用いた．通信ユニットには，USB 電源からの電力供給によりバッテリを充電する回路を搭載した．A/D 変換は，標本化周波数 1 kHz，分解能 12 bit で行う．

Bluetooth 通信には，Bluetooth 2.0+EDR の Serial Port Profile を用いた．通信速度は，心電図と脈波のデータ量から 40 kbps 以上の通信速度が必要であることを考慮して，115.2 kbps を選択した．十分な通信速度であり，計測データのオンライン通信が可能である．

心電図プローブは，小型の電極と信号処理回路から成る．電極は，生体計測に適した円盤状の Ag-AgCl を用いた．電極数は，差動増幅用の 2 極（LA，RA）とグラウンド用の 1 極（RF）の計 3 極である．電極の配置を図 4 (b) に示す．本研究の手法で必要な心電図波形は R 波のみのため，電極の装着可能な範囲は広く，左胸部付近で計測が可能である．なお，本センサでは心電図計測で用いられている標準 12 誘導のうち I 誘導と同様の波形が計測される．電極で計測された信号は，信号処理回路で増幅，アンチエイリアス処理される．

脈波プローブは，赤外発光ダイオード（LED: Light Emitting Diode），フォトダイオード（PD: Photodiode），信号処理回路から成る．LED の波長は 940 nm である．この波長は，血液での吸光度が高く，他の生体組織での吸収度が低いため，光電脈波計測に適している．LED と PD は，指に取り付けやすくするため，同一平面上に設置した．脈波信号も心電図信号と同様に増幅，アンチエイリアス処理される．

2・2・2 計測ソフトウェア

計測ソフトウェアの主な機能は，データ収録と stPWV の算出・表示である．これに付随する機能として，センサデバイスの制御，収録したデータの波形表示・保存機能を持つ．計測にともなう操作は，氏名（もしくは ID），身長の入力と計測開始ボタンのクリックである．計測開始に伴いセンサデバイスとの Bluetooth 通信の確立，計測開始命令の送信，計測データの収録と波形の表示が 30 秒間行われ，stPWV が計算・表示される．収録時間は，計測が負担にならないことを考慮しつつ，安定して十分な数の心拍数が計測できるよう設定した．

次に，脈波の伝播時間の算出処理について述べる．本研究では，30 秒間で検出された複数の R 波と脈波の立ち上がり開始点（以後 P_{min} と表記）から求められる時間差の平均を脈波伝播時間とした．処理の順序は，R 波の検出，脈波の立ち上がり開始点の検出，R 波と P_{min} の時間差の算出である．R 波は一拍の間において電位が最高値の点とした．脈波の立ち上がり開始点は一拍の間において最小値の点とした．

また，計測の精度と再現性を確保するために，上記処理の他に次の処理を行った．心電図は，R 波の検出前に，呼吸や体動によって生じる低周波ノイズである基線変動を除去するため，ハイパスフィルタを通過させた．フィルタの遮断周波数は，心電図の計測に必要な周波数帯域の下限である 0.14 Hz[14]を十分満たすよう 0.1Hz とした．脈波波形は，P_{min} 検出の前処理として移動平均を 30 サンプル（30 ms）で行った．この移動平均は 14.8 Hz のローパスフィルタとして働く．安静時の心拍数が 60 拍(1 Hz)程度であり、PWV 計測には脈波の第 10 高調波までを含めばよいとされているため[15]，周波数帯域の余裕を考慮して遮断周波数が 14.8 Hz（約 90 拍）となる 30 サンプルの移動平均を行った．不正な伝播時間が算出されることを防ぐために，R 波の検出数が心拍数に換算して毎分 40 拍以下と毎分 120 拍以上の場合には，伝播時間を算出しない．さらに，得られたすべての R 波と P_{min} の時間差の平均値と標準偏差を計算し，平均値から標準偏差以上はなれている時間差を除外した．このとき，除外されなかった時間差の平均値を伝播時間とした．ただし，除外されなかった時間差が一定数以下であるときは伝播時間を算出しないこととした．

3. 開発装置による動脈硬化スクリーニング指標の計測実験

3・1 計測精度の検証

3・1・1 実験方法

開発した装置の計測精度を検証するために，stPWV のばらつきを調べる実験を行った．プローブの取り付けによって変化する血流・受光量等の影響および，体動等の短時間における身体の状態変化の影響を確かめる．

実験の被計測者は，健常者の成人 8 名（男性，23~25 歳）である．被計測者には、実験前に実験の目的と方法を説明し、計測の同意を得た．5 分以上の安静をとり，仰臥位で計測を行った．実験は一人につき連続して 10 回

の stPWV 計測を行った．計測ごとに心電図プローブと脈波プローブを取り付け直した．10 回の計測値から変動係数（CV: Coefficient of Variation）を求め評価した．

3・1・2 実験結果

被計測者ごとの stPWV の平均値と標準偏差を図 5 に示す．表 1 に被計測者ごとの計測結果を示す．表中の L は伝播距離，SD は標準偏差，CV は変動係数である．

CV は，最小が 1.25 %，最大が 4.41 %，平均値が 2.34 %であった．既存の動脈硬化のスクリーニング指標の CAVI は，CV が 3.8 %程度で十分小さいとされている[16]ことから，stPWV の計測精度は十分小さく，従来と同程度以上の水準である．したがって，プローブの取り付けと短時間での身体の状態変化に起因する計測値のばらつきは実用に十分な水準といえる．

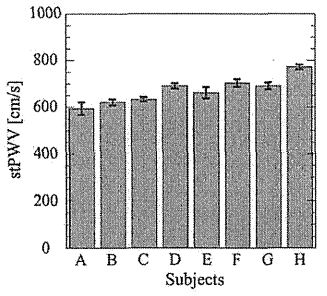

Fig. 5 Measurement results of stPWV

Table 1 Measurement results of stPWV

Subjects	Height [cm]	L [cm]	stPTT		stPWV		
			Mean [ms]	SD [ms]	Mean [cm/s]	SD [cm/s]	CV [%]
A	170	185.5	312.7	13.80	594.4	26.24	4.41
B	182	195.3	314.3	6.33	621.6	12.46	2.01
C	170	185.5	293.3	4.08	632.7	8.99	1.42
D	160	177.4	257.1	4.03	690.2	10.91	1.58
E	174	188.8	285.9	9.95	661.1	23.77	3.60
F	168	183.9	261.5	6.07	703.6	16.41	2.33
G	170	185.5	268.5	5.53	691.2	14.51	2.10
H	172	187.1	242.4	3.07	772.2	9.65	1.25

3・2 動脈壁の硬さとの対応関係の検証

3・2・1 実験方法

開発した装置で計測した stPWV が下肢の動脈の硬さに対応することを検証するための実験を行った．生体内にあるため動脈の硬さを直接計測することは困難である．そこで、大動脈 PWV と baPWV の比較方法[11]を基に、既に臨床応用されている動脈壁の硬さの指標と stPWV を比較する方法を用いた．比較対象には，計測対象の動脈が stPWV とほぼ等しい CAVI を用いた． CAVI と stPWV をほぼ同時に計測し，比較することで検証した．CAVI

は，haPWV を用いた指標であり，図 1 の haPWV の経路に対応する指標である．CAVI は動脈硬化のスクリーニングのための検査として医療機関で利用されてきている[10]．

CAVI の計測には，血圧脈波検査装置（VaSera，フクダ電子株式会社）を用いた．本実験では幅広い範囲の動脈の硬さと stPWV の関係性を調べることが目的であるため，疾患の有無や年齢によって被計測者の除外等は基本的に行わなかった．ただし、血圧についてのみ被計測者の条件として計測時の最高血圧が 18 kPa（135 mmHg）以下であることとした．被計測者は，男女 28 名（22~81 歳）である．被計測者には、実験前に実験の目的と方法を説明し、計測の同意を得た．計測は 5 分以上の安静をとり仰臥位で行った．CAVI の計測時にはカフによる圧迫が行われ血流が減少もしくは滞るため，stPWV と完全に同時の計測は行えない．そのため，stPWV は CAVI 計測の直後に計測した．CAVI の計測は，VaSera の動脈硬化のスクリーニング用の標準的な設定で行った．stPWV の計測手順は，3 章 1 節と同様に行った．CAVI と stPWV の結果の相関関係を調べた．

3・2・2 実験結果

図 6 に CAVI と stPWV 計測結果の関係を示す．被験者ごとにプロットした．

CAVI と stPWV の相関係数は，$r=0.707$ $(p<0.001)$となり，有意な相関関係を示した．相関係数が 0.7 以上であることから[17]，高い相関が示された．

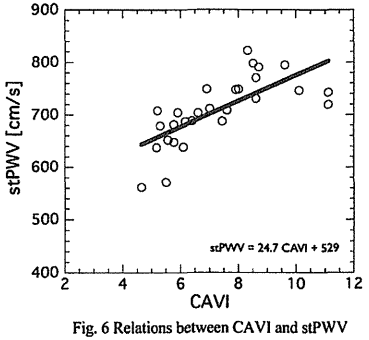

Fig. 6 Relations between CAVI and stPWV

4. 考察

本研究では，日常的な動脈硬化スクリーニング指標の計測を実現するための装置の開発を行った．開発した装置よって，心電図と光電脈波を用いた stPWV を計測できた．計測実験により，stPWV の精度が十分であることおよび動脈壁の硬さに対応することを確かめた．

計測精度の実験結果では，取り付け誤差や短時間での身体の状態変化によって，stPWV が大きな影響を受けないことを確かめた．取り付けの位置による心電図や脈波に振幅の変化は，特徴点の検出に対して影響が少ないと考えられる．また，短時間における身体の状態変化として，体動，心拍数，血圧が考えられるが，安静状態であればこれらの影響も少ないと考えられる．stPWV の CV は平均 2.34 %であり十分に小さいが，本研究では連続した計測での短期的な評価にとどまっている．身体状態は時間帯等によっても変化するため，今後は数時間から数日程度での評価を行い十分な精度を確保することが必要であると考えている．

stPWV の動脈壁の硬さに対応することを検証する実験では，相関係数が $r=0.707$ の高い相関を stPWV と CAVI の間に確認できた．既存の医療機関で計測されている動脈硬化のスクリーニング指標である baPWV と CAVI の間の相関係数は，$r=0.64$[18]から $r=0.88$[19]との報告がある．したがって，stPWV と CAVI の相関関係は，baPWV と CAVI の相関関係と同程度であり，動脈硬化スクリーニング指標として stPWV を用いることができる可能性が示唆された．

動脈壁の硬さとの対応関係の検証実験では，計測対象者を正常血圧値の者とした．これは，一般に PWV が血圧に対して依存性を持つ[20]一方で，CAVI が血圧に対して依存性の小さい指標である[11]ためである．血圧への依存性を除去するか否かは，気質的な動脈の硬さで評価する方法と機能的な（見かけ上での）硬さで評価するかによって異なる．本研究では，機能的な硬さの計測が動脈硬化の予防や治療効果の評価に有用であると考え，血圧による補正は行わなかった．さらに，血圧による補正を行った場合には，補正後の指標が血圧計の計測精度や計測誤差の影響を受けるため，厳密な血圧計測が必要で利便性が損なわれる可能性が高い．血圧による補正を行わない場合には，血圧計が不要なためシステムをより簡便にすることができる．正常血圧値の場合には血圧での補正なしでも CAVI と相関するため，正常血圧値の場合には stPWV をそのまま動脈硬化の予防・治療のための参考情報として活用できると考えられる．しかし，高血圧症は動脈硬化と密接に関わる疾患であるから，血圧が高い場合にも stPWV が適応できることを検証する必要がある．また，高血圧症に限らず動脈硬化と関連する疾患と stPWV の関係を調べる必要があると考えられる．

動脈壁の硬さとの対応関係の検証実験は，基礎的な stPWV の検証として幅広い範囲の動脈の硬さと stPWV の関係性を調べるために，疾患の有無や年齢によって被計測者の選別を行わなかった．しかし，stPWV によって、動脈硬化患者と健常者を見分けることができるかどうかや年齢による影響を分離することは，動脈硬化の診断・治療に用いる指標として重要である．したがって、stPWV について動脈硬化患者に対する計測や年齢による計測値の変化を考慮した計測を行い，その性質をさらに詳しく検証することが今後の課題である．

stPWV の計測対象は，上行大動脈から足の指の末梢動脈までである．この区間では，閉塞性動脈硬化症が生じやすい部位の一つである下肢の情報を得られるが，他の閉塞性動脈硬化症が生じやすい部位である頸動脈や冠状動脈の情報は直接得られない．しかし，全身の各部における PWV は互いにある程度の相関関係があり，加えて stPWV の経路には大動脈 PWV の計測対象の部位が含まれている．大動脈 PWV は，10 年間の心血管系疾患の発症リスクに相関することが報告されている[21]．したがって，stPWV では直接得られない部位の動脈硬化であっても，stPWV を観察することで間接的にその状態を観察できると考えられる．

さらに，stPWV 計測により従来の非侵襲な動脈硬化のスクリーニング指標である AI（Augmentation Index）[22]や ABI（Ankle Brachial Pressure Index）[23]を代替することができると考えられる．まず，stPWV と AI の関係について述べる．AI は脈波の波形のパラメータをもとに，動脈系の反射係数を動脈の硬さの指標としたものである．脈波の計測が 1 カ所で PWV よりもセンサが少ないが，原理的に心機能と動脈壁の特性の分離が難しい[22]．心機能を評価して，影響を除外するためには，心電図や心音の計測が必要となる．AI と心電図の計測は，脈波と心電図の計測となるため，stPWV の計測とほぼ同じ計測システムとなる．したがって，stPWV の計測情報をもとに AI と簡易的な心機能の評価を行うことも可能であると考えられる．AI は，動脈系全体の評価が可能であるから，stPWV の情報を AI の算出によって補完できると考えられる．次に，stPWV と ABI の関係について述べる．ABI は閉塞性動脈硬化症の診断に用いられている動脈の狭窄・閉塞の指標である．ABI が小さいほど，狭窄・閉塞による足首の血圧低下が大きい．重度の狭窄・閉塞が生じると baPWV や haPWV の値が見かけ上小さく（動脈が柔らかく）なるため，baPWV 等の信頼性を確保するために，ABI は baPWV 等と併用されている[24]．計測値の低下は PWV の原理的に生じるため，stPWV でも生じると考えられる．しかし，stPWV においては ABI を併用しなくても，信頼性を確保できると考えられる．閉塞・狭窄は動脈硬化の進行によって生じるため，重度の狭窄・閉塞の前に stPWV が上昇すると考えられる．すなわち，stPWV が上昇の後に下降するような変化を捉えることで狭窄・閉塞を検出できると考えられる．この手法の確立のためには，大規模で長期的な計測が必要となる．

上記の様な新たな計測値の評価方法を確立するためや計測値を診断や治療の参考情報として活用するためには，社会的なインフラの整備が必要であり、そのための stPWV を蓄積・管理・閲覧することのできるシステムの構築等の研究開発が必要となってくる．システム構築の一つとして，ネットワークやクラウド技術を応用した健康管理システムと stPWV の計測装置が連携してゆくことが有用であると考えられる．

5. 結論

本研究では，日常的な動脈硬化スクリーニング指標の計測を実現するために，センサが取り付け易く非拘束で計測できる簡便な装置を開発した．開発した装置のセンサデバイスは，被計測者自身で取り付けが可能で，計測時に被計測者を拘束しないため簡便である．開発した装置によって計測した stPWV が CAVI と同様に動脈硬化に関連する動脈壁の硬さと対応することを確かめた．stPWV の計測精度は十分高く， stPWV と CAVI が高相関を示した．

本研究では，被験者を血圧値で限定し，stPWV と動脈壁の硬さとの対応を調べた．今後は，stPWV と他の生体情報や疾患との関連性を検証し有効性を確かめることが必要である．また，操作性の向上や計測時間の短縮によって，さらに日常的に利用しやすい装置の開発および，地域医療や健康管理システムと連携する装置の開発が重要である．大規模で長期的な計測が可能なシステムを構築することで，総合的で継続的な動脈硬化の予防や治療を行うためのシステムへと本研究を展開させることができると期待できる．

謝　辞

本研究の一部は，文部科学省グローバル COE プログラム「サイバニクス：人・機械・情報系の融合複合」ならびに，内閣府最先端研究開発支援プログラム「健康長寿社会を支える最先端人支援技術研究プログラム」の支援により行われた．

文　献

(1) Mendis, S., Puska, P., Norrving, B., *Global Atlas on cardiovascular disease prevention and control* (2011), pp. 2-3, the World Health Organization in collaboration with the World Heart Federation and the World Stroke Organization.
(2) 岩井武尚，中島里枝子，“バスキュラーラボの役割と現況”，脈管学, Vol. 45, No. 5 (2004), pp. 285-289.
(3) Sugawara, J., Hayashi, K., Yokoi, K., Cortez-Cooper, M.Y., DeVan, A.E., Anton, M.A., Tanaka, H., “Brachial–ankle pulse wave velocity: an index of central arterial stiffness?”, *Journal of Human Hypertension*, Vol. 19, No. 5 (2005), pp. 401-406.
(4) Tanaka H, Munakata M, Kawano, ”between carotid-femoral and brachial-ankle pulse wave velocity as measures of arterial stiffness”, *Journal of Hypertention*. Vol. 27. No. 10 (2009), pp. 2022-0227.
(5) Yambe, T., Yoshizawa, M., Saijo, Y., Yamaguchi, T., Shibata, M., Konno, S., Nitta, S., Kuwayama, T., “Brachio-ankle pulse wave velocity and cardio-ankle vascular index (CAVI)”, *Biomedicine & Pharmacotherapy*, Vol. 58, No. 1 (2004), pp. 95-98.
(6) An-Bang, L., Po-Chun, H., Zong-Li, C., Hsien-Tsai, W., “Measuring pulse wave velocity using ECG and photoplethysmography”, *Journal of Medical Systems*, Vol. 35, No. 5 (2011), pp. 771-777.
(7) Nitzan, M., Khanokh, B., Slovik, Y., “The difference in pulse transit time to the toe and finger measured by photoplethysmography”, *Physiological Measurement*, Vol. 23, No. 1 (2002), pp. 85-93.
(8) Loukogeorgakis, S., Dawson, R., Phillips, N., Martyn, C.N., Greenwald, S.E., “Validation of a device to measure arterial pulse wave velocity by a photoplethysmographic method”, *Physiological Measurement*, Vol. 23, No. 3 (2002), pp. 581-596.
(9) 日本動脈硬化学会編，動脈硬化性疾患予防ガイドライン 2012 年度版, (2012), pp. 20-21，日本動脈硬化学会.
(10) 折茂肇，斎藤康監修，新しい動脈硬化指標 CAVI のすべて，(2009)，pp. 34-42，日経メディカル開発.
(11) 宗像正徳編, PWV を知る PWV で診る, (2006), pp. 21-26，中山書店.
(12) Yamashina, A., Tomiyama, H., Takeda, K., Tsuda, H., Arai, T., Hirose, K., Koji, Y., Hori, S., Yamamoto, Y. “Validity, Reproducibility, and Clinical Significance of Noninvasive Brachial-Ankle Pulse Wave Velocity Measurement”, *Hypertension Research*, Vol. 25, No. 3 (2002), pp. 359-364.
(13) 工業技術院 製品科学研究所, “AIST 人体寸法データベース 1991-92 TOP＞寸法項目検索＞統計量（M18）”, AIST 人体寸法データベース 1991-92, http://riodb.ibase.aist.go.jp/dhbodydb/91-92/data/search13.html（参照日 2013 年 5 月 17 日）
(14) 金井寛，生体計測学，(2009)，p. 28，コロナ社.
(15) Harold, S., Thomas, J.C., Sakti, M., Robert, A.W., “Effect of age on arterial distensibility in Asymptomatic humans”, *Arteriosclerosis, Thrombosis, and Vascular Biology*, Vol. 3, No. 3 (1983), pp. 199-205.

(16) Shirai, K., Utino, J., Otsuka, K., Takata, M., “A novel blood pressure–independent arterial wall stiffness parameter; cardio-ankle vascular index (CAVI)”, *Journal of Atherosclerosis and Thrombosis*, Vol. 13, No. 2 (2006), pp. 101-107.
(17) ジェラルド・G・シュッテ，統計学入門，(1981)，pp. 88-89，東洋経済新報社.
(18) Izuhara, M., Shioji, K., Kadota, S., Baba, O., Takeuchi, Y., Uegaito, T., Mutsuo, S., Matsuda, M. “Relationship of Cardio-Ankle Vascular Index (CAVI) to Carotid and Coronary Arteriosclerosis”, *Circulation Journal*, Vol. 72, No. 11 (2008), pp. 1762-1767.
(19) Takaki, A., Ogawa, H., Wakeyama, T., Iwami, T., Kimura, M., Hadano, Y., Matsuda, S., Miyazaki, Y., Hiratsuka, A., Matsuzaki, M., “Cardio-Ankle Vascular Index Is Superior to Brachial-Ankle Pulse Wave Velocity as an Index of Arterial Stiffness”, *Hypertension Research*, Vol. 31, No.7 (2008), pp. 1347-1355.
(20) Yamashina, A., Tomiyama, H., Arai, T., Koji, Y., Yambe, M., Motobe, H., Glunizia, Z., Yamamoto, Y., Hori, S., “Nomogram of the relation of brachial-ankle pulse wave velocity with blood pressure”, *Hypertension Research*, Vol. 26, No. 10 (2003), pp. 801-806.
(21) Blacher, J., Asmar, R., Djane, S., London, G. M., Safar, M. E., “Aortic pulse wave velocity as a marker of cardiovascular risk in hypertensive patients”, *Hypertension*, Vol. 33, No. 5 (1999), pp. 1111-1117.
(22) 宗像正徳編，PWV を知る PWV で診る，(2006)，pp. 239-246，中山書店.
(23) Thom, W.R., Alan, T.H., Sanjay, M., Anton, N.S., Joshua, A.B., Laura, K.F., Jafar, G., Heather, L.G., Jonathan, L.H., Michael, R.J., Gregory, L.M., Jeffrey, W.O., James, C.S., Christopher, J.W., John, V.W., R., Eugene, Z., “2011 ACCF/AHA Focused Update of the Guideline for the Management of Patients With Peripheral Artery Disease (Updating the 2005 Guideline) a report of the American College of Cardiology Foundation/American Heart Association Task Force on Practice Guidelines”, *Journal of the American College of Cardiology*, Vol. 58, No. 19 (2011), pp. 2020-2045.
(24) Motobe, K., Tomiyama, H., Koji, Y., Yambe, M., Gulinisa, Z., Arai, T., Ichihashi, H., Nagae, T., Ishimaru, S., Yamashina, A., “Cut-Off Value of the Ankle-Brachial Pressure Index at Which the Accuracy of Brachial-Ankle Pulse Wave Velocity Measurement is Diminished”, *Circulation journal*, Vol. 69, No. 1 (2004), pp. 55-60.